UNIVERSITY OF CALIFORNIA, SAN DIEGO

Microstructure and Mechanical Property Comparison of Different Keratinous Horns

A thesis submitted in partial satisfaction of the requirements

for the degree Master of Science

in

Materials Science and Engineering

by

Yuchen Zhang

Committee in charge:

Professor Joanna M. McKittrick, Chair
Professor Shengqiang Cai
Professor Michael T. Tolley

2017

The Thesis of Yuchen Zhang is approved, and it is acceptable in quality and form for publication on microfilm and electronically:

Chair

University of California, San Diego

2017

TABLE OF CONTENTS

Signature Page iii

Table of Contents iv

List of Figures vi

List of Tables ix

Acknowledgements x

Abstract of The Thesis xi

1 Introduction 1

2 Background 4

2.1 Keratin 4

2.1.1 Structure of Keratin 4

2.1.2 Humidity Sensitivity of Keratin 9

2.1.3 Mechanical Properties of Keratin 12

2.2 Impact Resistant Natural Materials 17

2.3 Horn Structure and Mechanical Behavior 20

2.4 Fighting Behavior 24

3 Hypotheses 27

4 Materials and Methods 28

4.1 Optical Microscopy 28

4.2 Scanning Electron Microscopy (SEM) 28

4.3 Water Absorption Test 29

4.4 Porosity Measurement 30

4.5 Compression Test 30
4.6 Tensile Test 32
4.7 Impact Test 33
5 Results and Discussion 37
5.1 Structural Characterization 37
5.2 Mechanical Properties 44
5.2.1 Compression Test 44
5.2.2 Tensile Test 57
5.2.3 Impact Test 61
6 Conclusions 65
7 Recommendations for Future Research 69
Appendix 70
Appendix I. Optical Microscopy Sample Preparation Protocol 70
References 72

LIST OF FIGURES

Figure 1. Toughness versus Young's modulus map showing mechanical properties of biological materials. Keratin is shown in the red oval. Taken from [2]. 2

Figure 2. (a) Two α-helical chains coiled-coil assemble, forming a heterodimer. (b) Schematic drawing of a heterodimer, taken from [27, 41]. 6

Figure 3. Schematic diagram of the hierarical structure of intermediate filaments. Taken from [37]. 6

Figure 4. Transmission electron microscopy image of a ram horn [37]. The dark strand is an intermediate filament and the lighter part is the amorphous matrix. 7

Figure 5. Molecular component of β-keratin [9, 32]. The central domain forms a β-sheet and N- and C-ends forms the matrix. The central domain is formed by a polypeptide chain folding several times forming a pleated sheet structure..... 8

Figure 6. X-ray diffraction patterns of (a) α-keratin and (b) β-keratin [9]..... 9

Figure 7. Water interaction with matrix proteins. Taken from [46]: **(I)** water act as a cross-linker and swelling agent to increase the space between chains, **(II)** water molecules replace secondary hydrogen bonds between chains and **(III)** water interacts with matrix proteins forming a network..... 11

Figure 8. The transformation from α-helix to β-sheet when applying tensile stress to α-keratin, taken from [48]. 14

Figure 9. Atomic simulation of the tensile force-displacement curves for **(a)** heterodimer, **(b)** tetramer without disulfide cross-links and **(c)** tetramer with disulfide cross-links. Taken from [58]..... 16

Figure 10. **(a)** Photograph of the bighorn sheep horn; **(b)** microstructure of the horn (perpendicular to growth direction); **(c)** hierarchical structure of the horn. (d) schematic diagram of single keratin cell and cell arrangement. Adapted from [17]. 21

Figure 11. Three points bending stress-strain curves of samples obtained from different parts along the cattle horn. Taken from [70]..... 22

Figure 12. Stress-strain curves of cattle horn under tensile test; three hydration levels of sample were tested. Taken from [70]. 23

Figure 13. Scanning electron micrographs of the fracture surface of ambient dry bighorn sheep horn after three-point bending test. Taken from [17]..... 24

Figure 14. Combat style and external horn morphology of four species: **(a)** bighorn sheep, **(b)** domestic sheep, **(c)** mountain goat and **(d)** pronghorn. 26

Figure 15. Compressed sample and the cutting position. Compressive load was applied in the longitudinal direction. After compression, samples were prepared by cutting samples parallel to the longitudinal direction. 29

Figure 16. Three orthogonal orientations defining the horns. All compressive test samples were cut from the central region. 31

Figure 17. Schematic diagram of the modified impact test machine, showing the sizes of each component, taken from [22]. 34

Figure 18. Low magnification optical micrographs of horn slices perpendicular to the longitudinal direction. 38

Figure 19. Fracture surface of pronghorn horn broken in LN_2. A tubule with fiber pulled out is shown in the left and hair like fiber bundle is shown in the right. 39

Figure 20. High magnification optical micrographs of horn slices perpendicular to the longitudinal direction. Keratin cells are shown for **(a)** bighorn sheep, **(b)** domestic sheep, **(c)** mountain goat and **(d)** pronghorn. 40

Figure 21. Optical micrographs of longitudinal sections of the horns. 41

Figure 22. High magnification optical micrographs of the longitudinal sections. Keratin cells of **(a)** bighorn sheep and **(b)** domestic sheep turn to have more sharp arcs and protuberances. Cells of the **(c)** mountain goat and **(d)** pronghorn are thinner with a more regular oval shape. 42

Figure 23. Water content (wt.%) of horns both in the ambient and fully rehydrated conditions. Water content of different horns is similar under ambient environment. When fully rehydrated, the pronghorn has a significantly larger water content than the other horns. 43

Figure 24. Scanning electron micrographs of the longitudinal cross-sections. **(a)** There are nanopores in pronghorn keratin cells. No obvious voids are observed in the cells of the **(b)** mountain goat, **(c)** bighorn sheep and **(d)** domestic sheep. 44

Figure 25. Compressive stress-strain curves comparison of different ambient dry horns in **(a)** longitudinal direction, **(b)** radial direction and **(c)** transverse direction. (n = 5) 45

Figure 26. Scanning electron microscopy images showing inner sections of the bighorn sheep horn after 70% compression. 48

Figure 27. Scanning electron microscopy images showing inner sections of domestic sheep horn after 70% compression. **(a)** Image near the side surface of the specimen and **(b)** near the mid-section of the specimen. **(c)** Delamination and fiber bridging are shown. 49

Figure 28. Scanning electron microscopy images showing inner sections of the mountain goat horn after 70% compression. 50

Figure 29. Scanning electron microscopy images showing inner sections of pronghorn horn after 70% compression. **(a)** Near the side surface of the specimen and **(b)** near the mid-section. **(c)** Delamination and fiber bridging are observed. 51

Figure 30. Compressive stress-strain curves comparison of rehydrated horns in the **(a)** longitudinal, **(b)** radial and **(c)** transverse directions. The yield and ultimate strength of the pronghorn horn is much smaller than the other horns. (n = 5) 52

Figure 31. Energy absorption with the compressive strain of dry and rehydrated horns in the **(a)** longitudinal, **(b)** radial and **(c)** transverse directions. (n = 5) ... 55

Figure 32. The changes of (a) Young's modulus, (b) yield strength, (c) resilience and (d) toughness associated with the water content of different horns in longitudinal, radial and transverse directions. 56

Figure 33. Average (n = 7) longitudinal tensile stress-strain response for the horns. Specimen are in the ambient dry condition..... 58

Figure 34. Scanning electron microscopy images of tensile fracture surfaces of the horns. The left are low magnification images and the right are high magnification images. **(a,b)** big horn sheep, **(c,d)** domestic sheep **(e,f)** mountain goat and **(g,h)** pronghorn. 60

Figure 35. Commonly observed damage modes after a drop tower test. NDI represents for non-destructive inspection method. Taken from [78]. 61

Figure 36. External damage modes of **(a)** and **(b)** domestic sheep and **(c)** and **(d)** bighorn sheep with associated normalized impact energy (E_n). Radial direction points out of the page. Black lines are from a pen..... 63

Figure 37. Damage types (bottom surface) with different normalized impact energy from the **(a)** domestic sheep and **(b)** bighorn sheep horn. 64

LIST OF TABLES

Table 1. Summary of the molecular units, dimensions and keratin assemblies of α- and β-keratins. (IF = intermediate filament) 8

Table 2. Keratin type and its distribution. 9

Table 3. Mechanical properties of α- and β-keratins. 12

Table 4. Chemical composition, hierarchical structure, mechanical properties of several structural biological materials and their biological functions of some natural materials. 18

Table 5. Porosity and average pore size of the different horns. 39

Table 6. Young's modulus, yield strength, resilience and toughness of ambient dry horns in three directions. 47

Table 7. Water content, Young's modulus, yield strength, resilience and toughness of fully rehydrated horns. 53

Table 8. Longitudinal tensile mechanical properties of ambient dry horns. 58

ACKNOWLEDGEMENTS

First I want to acknowledge Professor Joanna McKittrick for her support and intellectually stimulating ideas on my thesis project, and be the chair of my thesis committee. I also want to thank Professor Cheryl Hayashi at UC Riverside for helpful discussions and providing the mountain goat horns.

I also want to acknowledge the contribution of the following individuals and groups who have helped me in immeasurable ways: Professor Michael T. Tolley and Professor Shengqiang Cai of Mechanical and Aerospace Engineering department for being on my thesis committee; Ryan Anderson of Nano3 Clean Room for giving technical support on using optical microscopes and scanning electron microscope; Ying Jones from Cellular and Molecular Research Department for providing machine Leica Ultracut UCT Ultramicrotome and technical support on preparing ultra-thin samples; lab mate Wei Huang and Daniel Yu from Professor Meyers's group for assisting me in performing quasi-static mechanical tests and lab mate Keisuke Matsushita for helping me with drop weight tests. I also want to acknowledge my fellow lab members, Frances Yenan Su, Jerry (Jae-Young) Jung and Michael B. Frank, for their inspiring comments and expertise in experimental methods. Finally, I want to acknowledge my parents for their generous financial and spiritual support for my graduate studies.

This work was supported by a Multi-University Research Initiative through the Air Force Office of Scientific Research of the United States (AFOSR-FA9550-15-1-0009).

The thesis is currently being prepared for submission for publication with Yuchen Zhang as the first author.

ABSTRACT OF THE THESIS

Microstructure and Mechanical Property Comparison of Different Keratinous Horns

by

Yuchen Zhang

Master of Science in Materials Science and Engineering

University of California, San Diego, 2017

Professor Joanna M. McKittrick, Chair

This thesis investigates the microstructure and mechanical properties of horns from the bighorn sheep, domestic sheep, mountain goat and pronghorn, which are all composed of keratin. Microstructural similarity is found where disk-shaped keratin cells attach edge-to-edge along the tubule (medullary cavity) growth direction (longitudinal direction) forming a lamella, and the lamellae are layered face-to-face along the impact direction (radial direction), and forming a wavy pattern surrounding the tubules. Differences include the number and shape of the tubules, lamellae aligned direction and shape of keratin cells.

Water absorption test reveals that the pronghorn horn has the largest water absorbing ability due to the presence of nanopores in the keratin cells. Stress direction and hydration dependent anisotropic mechanical behavior is found as common characteristics of horns. The differences in the mechanical properties between horns of different species can be explained as facilitating their different fighting behaviors. Fracture surface examination proves similar deformation and fracture mechanisms, with microbuckling and delamination mechanism under compressive stress and fiber breakage mechanism under tensile stress, while crack length and fiber-to-fiber adhesion affect strength of the horns.

1 Introduction

The study of biological materials, including the study of chemical composition and structural organization, paves the road to invent new materials. Especially, biological materials with a simple chemical constituent but possessing excellent mechanical properties have drawn attention to scientists for some time. The toughness of a material is a measurement of its resistance to the propagation of cracks [1]. The Young's modulus is the stiffness of a solid material. The relationship between toughness and Young's modulus of natural materials is shown in the Wegst-Ashby map [2] (Figure 1). Being one of the toughest biological material, keratin also process a relatively high modulus, even though it is solely constituted of a biopolymer, some with a small mineral presence [3]. Keratinous materials are formed by hierarchical organized keratin cells with fibrous keratin as the main constituent of the cell [4]. The hierarchical structure of keratinous materials from the nanoscale to centimeter scale is: polypeptide chain structure [5, 6], filament-matrix structure [7-12], lamellar structure [13-17], and sandwich structure [18, 19]. Wool, feathers, claws, and beaks of birds and reptiles, and hooves and horns of mammals are all constituted of keratinous materials, and each of them serves functions such as protection (e.g. waterproof feathers), defense (e.g. pangolin scales) and predation (e.g. claws).

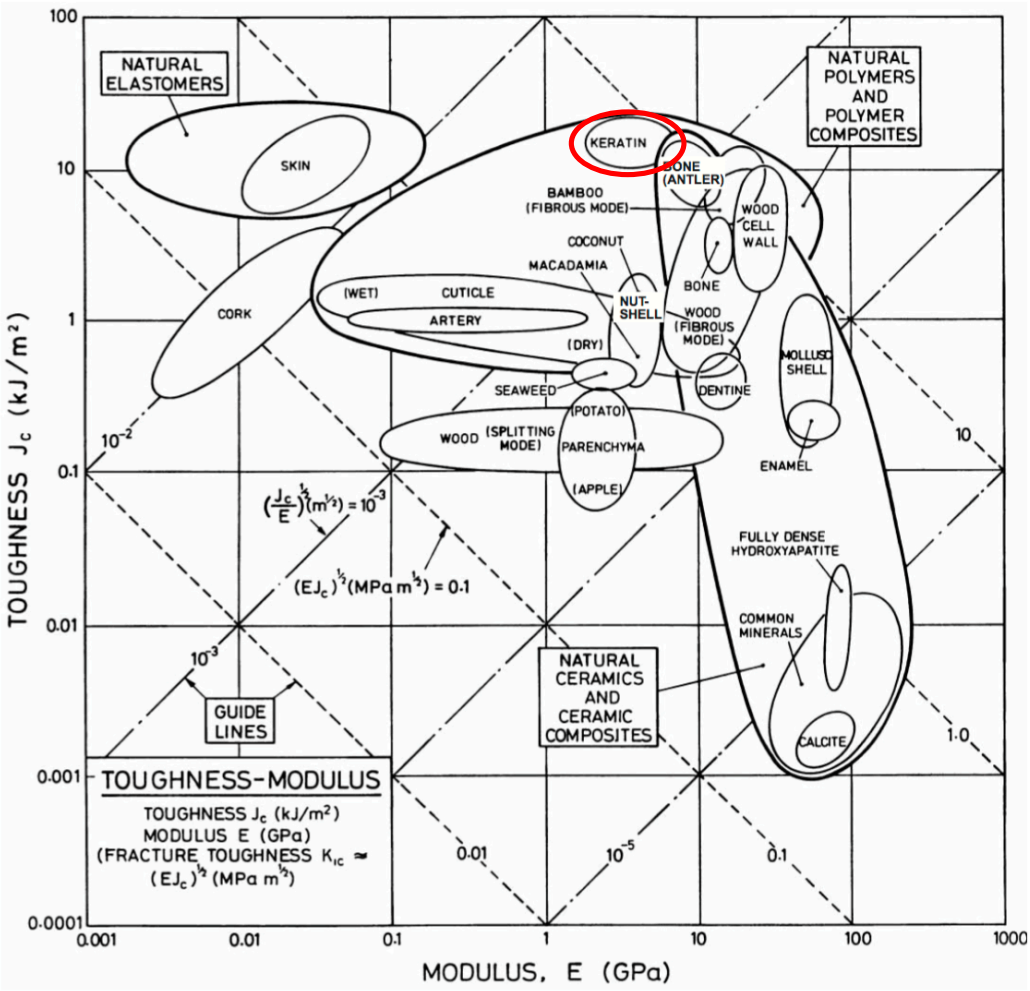

Figure 1. Toughness versus Young's modulus map showing mechanical properties of biological materials. Keratin is shown in the red oval. Taken from [2].

Keratinous horns of mammals, found mainly in the Bovidae family (e.g. cattle, sheep, goats, buffalo, antelope) and Antilocapridae family (e.g. pronghorn) act as attack and defense weapons during combat. Given the lifespan of mammals and the inability of most horns to regrow (the pronghorn is an exception), the horns must be resistant to fracture. As a main protection feature of the head during fights, the horns should be energy absorbent and impact resistant [20]. With the superior mechanical properties and durability,

the study of hierarchical structure of keratinous horns can provide principles and mechanisms for inventing novel safety and impact resistant materials.

Previous research has investigated microstructure and mechanical response under different stress state of bighorn sheep (*Ovis canadensis* [21]) horn [17, 22, 23]. However, the investigation of other horns in the Bovidae and Antilocapridae families has not been performed. Therefore, the horns investigated in this thesis are from four individual species: bighorn sheep, domestic sheep (*Ovis aries* [24]), mountain goat (*Oreamnos americanus* [25]) and pronghorn (*Antilocapra americana* [26]). Domestic sheep and bighorn sheep are close relatives with similar fighting behavior. The mountain goat has a relatively far relationship to the sheep and with a different fighting style. The pronghorn evolved a similar horn structure and fighting style with the Bovidae family.

The microstructure, mechanical properties and fracture mechanism of the different horns are studied to find structural influence on mechanical performance, further making correlation to their fighting behavior. The influence of hydration on mechanical properties is also investigated, to give guidance for future tuning of the mechanical performance of impact resistant materials.

2 Background

2.1 Keratin

Keratins are a group of insoluble and filament-forming proteins belonging to the superfamily of intermediate filament (IF) proteins [27]. Keratins are mainly produced in certain epithelial cells of vertebrates [28]. With the properties of being inert to the outside environment, long-lasting and tough, the main function of keratins is to give protection to epithelial cells from mechanical and non-mechanical stresses [28]. Based on X-ray diffraction, four patterns of keratins can be identified, which are α-pattern, β-pattern, feather pattern and amorphous pattern [9, 29-31]. The feather pattern keratin has been accepted to be considered as the β-pattern keratin, having same characteristic reflections as the β-pattern [32]. The amorphous pattern is found both in α- and β-keratinous tissues. Among the four patterns, α- and β-pattern distinguish the differences between keratinous materials. Associated with α- and β- keratins, there are two regular secondary structures, which are α-helices and β-sheets. Since α- and β-keratin mainly exist in its specific secondary structure, α-helices and β-sheets can be used to classify keratins [33].

2.1.1 Structure of Keratin

The monomeric unit of α-keratin is heterodimer, which is formed by a left-handed coiled-coil assembling of two isolated right-handed α-helical chains, by disulfide crosslinks [28], shown in Figure 2 (a). An α-helical chain contains a central α-helical rod and non-helical N- and C-terminal domains. The N- and C- terminal domains have the function of bonding with other IFs and the matrix. There are also three non-helical links on

the central rod, which are termed L1, L12 and L2 [34]. A schematic diagram of the heterodimer is shown in Figure 2 (b). A single heterodimer has a length of 45 nm, excluding non-helical terminals [35]. The diameter is about 2 nm [36]. There is a high content of glycine and alanine in heterodimer, and the high content of cysteine and half-cysteine provides disulfide cross-linked bonds. The disulfide bonds form sulfur cross links between two α-helical chains, making the heterodimer stiff and insoluble [17]. Heterodimers link each other with non-helical N- and C-ends to form protofilaments and then the protofilaments polymerize to form the IFs [37] (Figure 3). The IFs are embedded in an amorphous keratin matrix. The amorphous keratin contains two types of proteins, one is high-glycine-tyrosine protein and the other is high sulfur protein. The high glycine-tyrosine proteins contain high glycyl residues and the high sulfur proteins contain more cysteinyl residues [38]. The matrix can be described as an isotropic elastomer [39]. A transmission electron microscope (TEM) image (Figure 4) exhibits an IF and the surrounding amorphous matrix. In the figure, the dark thread is the IF and the lighter region is the amorphous matrix [40].

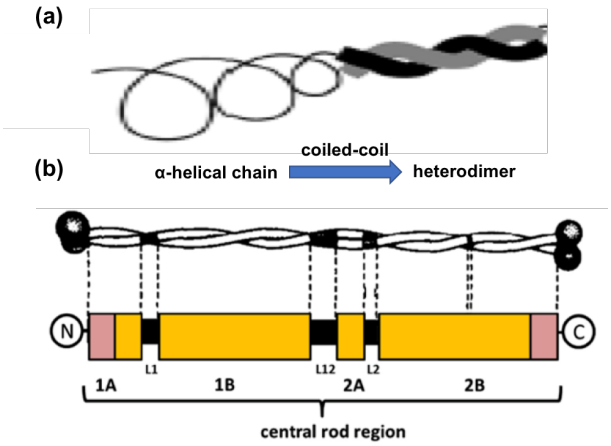

Figure 2. (a) Two α-helical chains coiled-coil assemble, forming a heterodimer. (b) Schematic drawing of a heterodimer, taken from [27, 41]. Non-helical N- and C-terminal domains bond with matrix or other intermediate filaments. The central region is α-helical coiled coil assembled with L1, L12 and L2 short links. 1A, 1B, 2A, 2B are α-helical coiled coil regions.

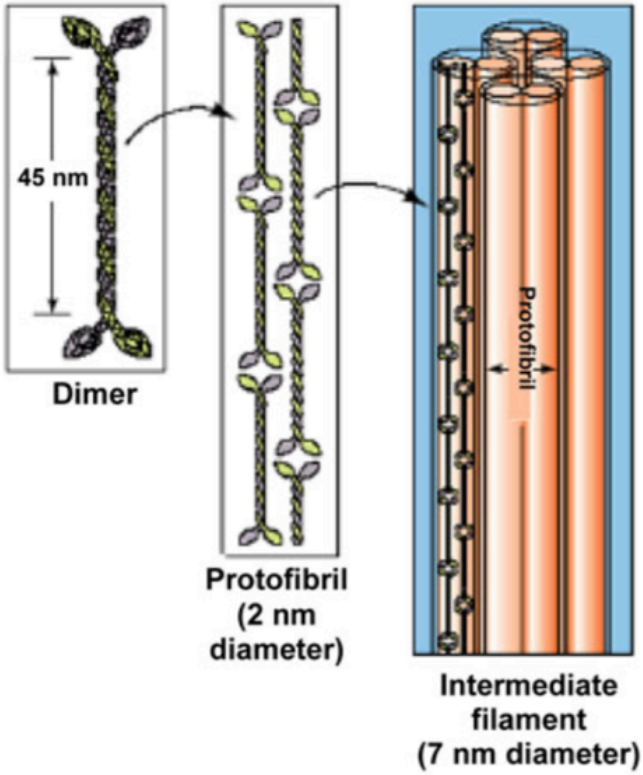

Figure 3. Schematic diagram of the hierarical structure of intermediate filaments. Taken from [37]. Two keratin polypeptides assemble to form a coiled coil to form a heterodimer. The heterodimer is assembled head to tail to form the protofilament. Protofilaments bimerize to form a protofibril and eight of protofibrils form an intermediate filament (IF).

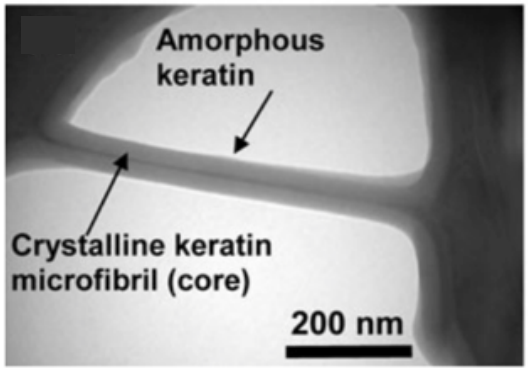

Figure 4. Transmission electron microscopy image of a ram horn [37]. The dark strand is an intermediate filament and the lighter part is the amorphous matrix.

The molecular component of β-keratin also contains three domains. Shown in Figure 5, the central domain is the section forming β-sheet and the N- and C-terminal domains are attached at the end of the central domain [9]. The central domain is formed by the central part of a polypeptide chain. The polypeptide chain folds several times forming a pleated sheet structure. The lateral parts of the chain form the N- and C-terminals [32]. The length of the central region is about 2.3 nm with a diameter about 2 nm [9]. The IFs of β-keratin are formed by a pleated sheet arrangement and the matrix is formed by N- and C-ends. The matrix surrounds the central domain, forming the β-keratin [32]. A summary of molecular units, dimensions and keratin assemblies of α- and β-keratins is shown in Table 1.

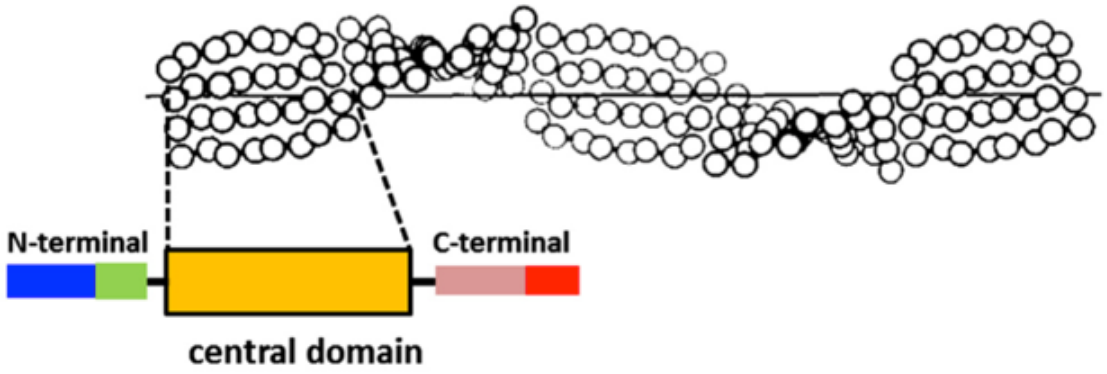

Figure 5. Molecular component of β-keratin [9, 32]. The central domain forms a β-sheet and N- and C-ends forms the matrix. The central domain is formed by a polypeptide chain folding several times forming a pleated sheet structure.

Table 1. Summary of the molecular units, dimensions and keratin assemblies of α- and β-keratins. (IF = intermediate filament)

Category	α-Keratin	β-Keratin
Molecular unit	Dimer	Distorted pleated sheet
Length of central molecular unit	45 nm [35]	2.3 nm [9]
Diameter of molecular unit	2 nm [36]	2 nm [9]
Assembling method	Dimers organize into IFs; N- and C-terminal domains link to matrix proteins or other IFs; matrix surrounds around IFs to form keratin [42].	IFs are formed by pleated sheet arrangement; N- and C-terminal domains form matrix; matrix surrounds around IFs to form keratin [32].

The X-ray diffraction patterns of α- and β-structures are shown in Figure 6. The diffraction pattern of α-keratin (Figure 6 (a)) has an equatorial reflection of spacing 0.98 nm and a meridional reflection of spacing 0.515 nm, which correspond to a 0.98 nm distance between α-helical axes and an α-helix pitch along the coiled coil axis contributed by side-chains configurations. The X-ray diffraction pattern of β-keratin is shown in Figure 6 (b). The pattern has equatorial reflections of spacing 0.97 nm and 0.47 nm, which

represent the distance between β-sheets and the distance between chains in one β-sheet, respectively. The meridional reflection of spacing 0.31 nm in β-keratin pattern represents the distance between residues (single amino acids) along a chain in the β-sheet [9, 31, 43, 44]. α-Keratin is the main component of wool, hair, horns and hooves and is mostly found in mammals. β-keratin is the main component of feathers, reptilian claws and scales, avian beaks and claws. Reptilian epidermis and pangolin scales have both α-keratin and β-keratin [45]. The keratin type and its main distribution are listed in Table 2.

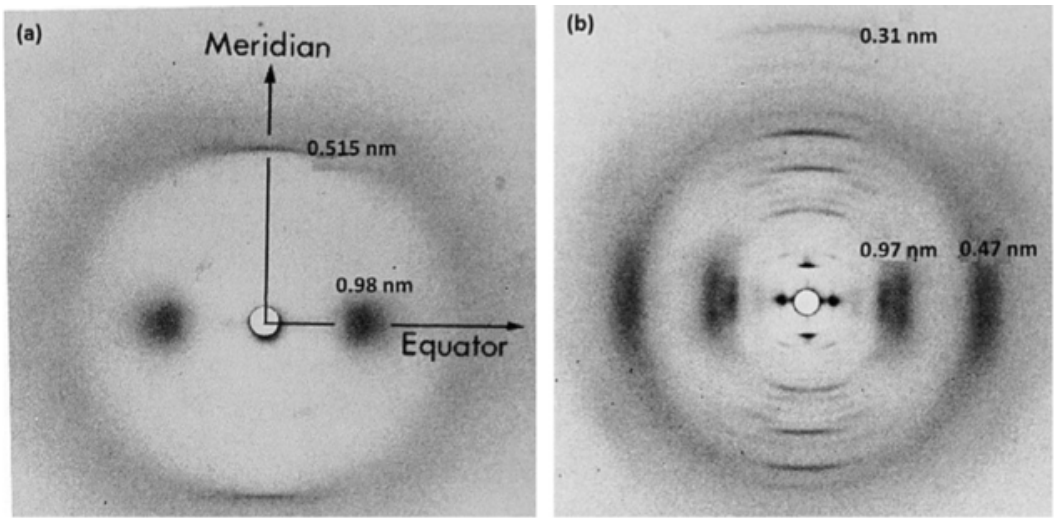

Figure 6. X-ray diffraction patterns of (a) α-keratin and (b) β-keratin [9].

Table 2. Keratin type and its distribution.

α-Keratin	Horns, hooves, wool, hair, fingernails, hagfish slime
β-Keratin	Feathers, reptilian claws and scales, avian beaks and claws
α- and β-Keratin	Reptilian epidermis, pangolin scales

2.1.2 Humidity Sensitivity of Keratin

Keratinous materials are highly sensitive to moisture. As the water content increases, the strength and stiffness decrease but the failure strain increases [46]. Previous

studies reveal that matrix is the main media absorbing water and since the IFs are crystalline, they are not affected [47]. Other studies show that hydrated IFs are quite soft, probably due to the elastomeric IF protein terminal domains in series with stiffer coiled coils [48]. Considering the matrix as the main component of water absorption, there are three ways how water molecules can connect to matrix proteins, illustrated in Figure 7. As shown in Figure 7 (I), the first way is that water molecules cross-link the α-chains. The water molecules act as a swelling agent and extend the space between chains, thus reducing the interaction between chains [47]. The second way (shown in Figure 7 (II)) is that water molecules may replace the secondary hydrogen bonding thereby increasing the protein mobility [49]. The final way (shown in Figure 7 (III)) is that water molecules and matrix proteins connect to form a network that acts as a plasticizer, thus the stiffness is reduced and mobility increased [47]. However, without the amorphous matrix, the IFs have been shown to be water sensitive from studies on hagfish slime. This implies that water affects structural bonds or the disordered region in IFs [50, 51].

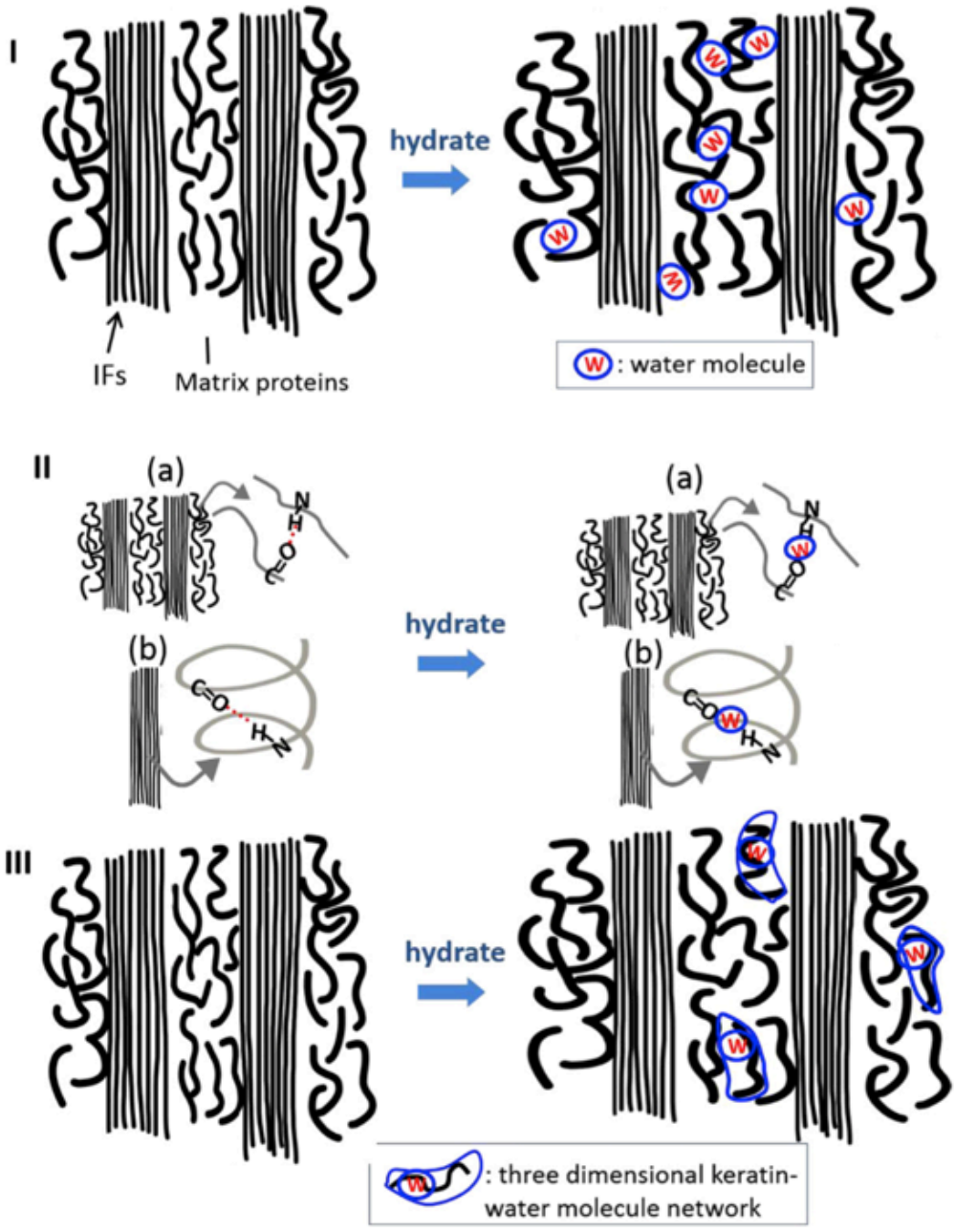

Figure 7. Water interaction with matrix proteins. Taken from [46]: **(I)** water act as a cross-linker and swelling agent to increase the space between chains, **(II)** water molecules replace secondary hydrogen bonds between chains and **(III)** water interacts with matrix proteins forming a network.

2.1.3 Mechanical Properties of Keratin

General information of mechanical properties of α- and β-keratins is summarized in Table 3. As shown, α-keratin is less stiff than β-keratin [52] and when α-keratin is under tensile stress, it will transform into β-sheets [53]. By mineralization with calcium and other salts, the stiffness of keratins increases [54]. The fraction and alignment of IFs vary among the materials and have an influence on mechanical properties. Hydration is also a factor affecting mechanical performance. When increasing humidity or water content, the strength and Young's modulus of both α-keratin and β-keratin decreases. For α-keratin, the Chapman/Hearle model has been considered fairly realistic [55]. In Chapman/Hearle model, the matrix is assumed to be a highly cross-linked swollen rubber and the IFs are considered as ideal α-helical crystals. The matrix has been modeled as an elastomer [56] and serves as a softer component to transfer stress to the stiffer fibers and therefore it can prevent crack propagation [57]. For β-keratin, there has been no model developed.

Table 3. Mechanical properties of α- and β-keratins.

α-Keratin is less stiff than β-keratin.
The α-helices with transform to β-sheets under tensile stress.
Mineralization increases the stiffness of α- and β-keratins.
Hydration decrease the strength and Young's modulus.
Orientation, packing and volume fractions of IFs affect mechanical properties.
The amorphous matrix is assumed to be elastomer while IFs are considered to be crystalline.
No common model has been developed for β-keratin.

Figure 8 shows the α-helix to β-sheet transformation under a tensile stress. Figure 8 (a) and (b) shows the X-ray diffraction pattern changes of hagfish thread under tension [48]. When the strain is > 30%, the IFs transform from the α-helix into the β-sheet. In the X-ray

diffraction pattern, the space between equatorial reflections changes to 0.97 nm and 0.47 nm, which obeys a typical β-keratin pattern. As shown in Figure 8 (c), the hydrogen bonds rearrange and the α-helix changes into β-sheet. When the IFs are unloaded, the space between central point and first equatorial reflection point is 0.98 nm and the space between central point and first meridional reflection point is 0.515 nm, which indicate the α-keratin pattern. There are three related regions exhibited in the stress-strain curve (Figure 8 (d)). At first at 2%-5% strain, a linear Hookean region exists, which refers to a change in bond arrangement of α-helices but without substantial structural changes. When strain is larger than 2%-5% but smaller than 30%-50%, a yield region is generated, which indicates a gradual transition progress from the α-helix to β-sheet by unraveling of the coiled coils. When strain is larger than 30%-50%, the curve steepens, which indicates that a large number of β-sheets are formed. The transformation from α-helix to β-sheet allows keratinous materials to absorb a large amount of energy without fracture. The energy absorbing ability, which is calculated by measuring the area under the stress-strain curve, is obviously enhanced. When the load is released, part of the energy (elastic) will be recovered [46].

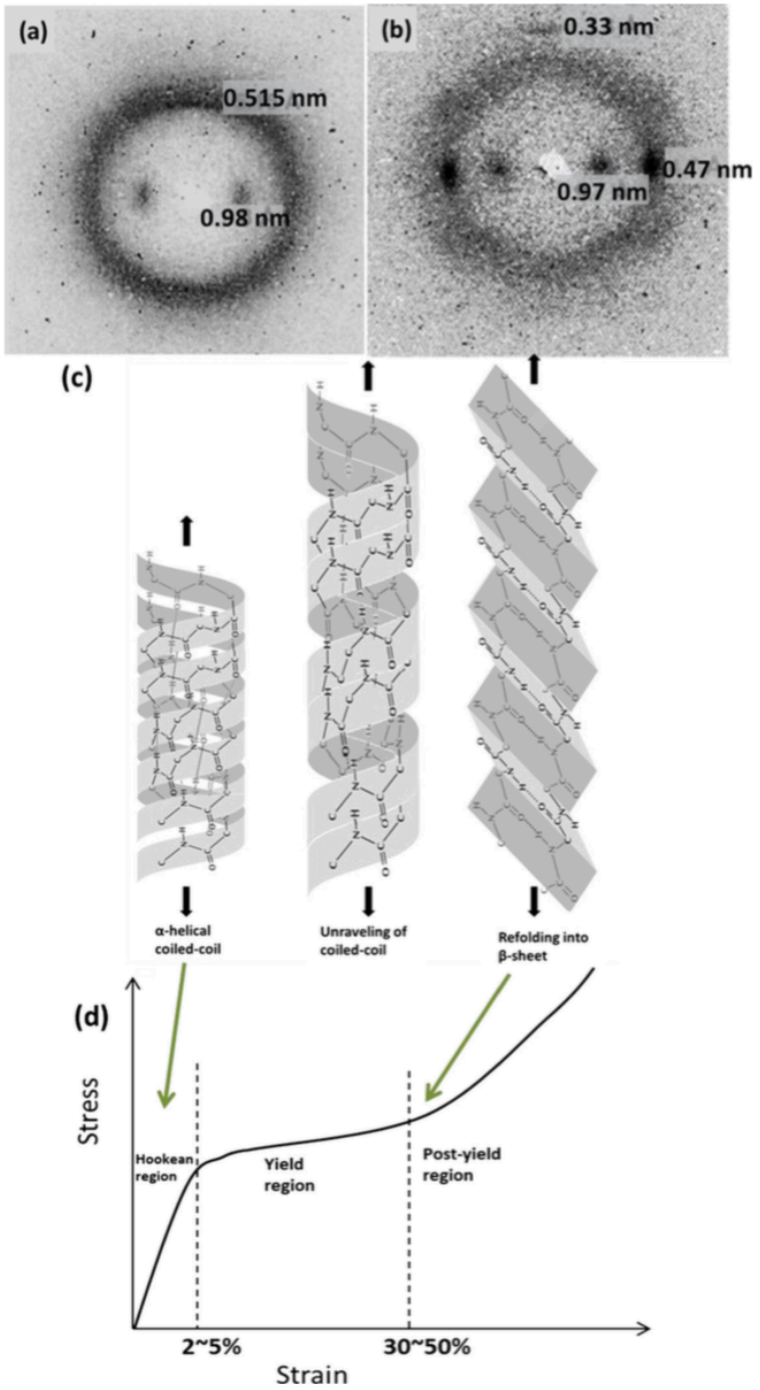

Figure 8. The transformation from α-helix to β-sheet when applying tensile stress to α-keratin, taken from [48]. **(a)** and **(b)** are X-ray diffraction pattern of hagfish thread before and after tension. **(c)** Schematic drawing showing the transformation of the α-helices into β-sheets. **(d)** Schematic diagram of the corresponding stress-strain curve.

The deformation behavior of α-keratin has been simulated at molecular scale [58]. The simulated tensile force-displacement curves of a heterodimer and truncated tetramers (formed by two heterodimers) [58] are shown in Figure 9. The curves are divided into three regions. In the low stress region, the force increases linearly with displacement (region I) due to stretching of the heterodimer, prior to cleavage of the hydrogen bonds and the α-helices uncoil. In region II, the α-helices starts uncoiling and the tensile force fluctuates. In region III, the tensile force increases significantly with displacement due to stretching of covalent bonds of the polypeptide chain backbone. The heterodimer will keep stretching until all α-helices are fully extended [58]. Since the cysteine and half-cysteine residues existing at the N- and C-terminals provide sufficient disulfide cross-linked bonds in keratin proteins, the study of mechanics of disulfide cross-links is important. Figure 9 (b) and (c) simulate tetramers without and with disulfide bonds, respectively. Region I is similar to the response of heterodimer, where the force increases linearly with displacement. But when the tetramer is without disulfide bonds, the force decreases in regions II and III. This phenomenon can be explained as the sliding and cleavage of hydrogen bonds in the tetramer. For a tetramer with disulfide cross-links, there is a peak in the force with the increasing of displacement, which indicates the rupture of disulfide cross-links between two dimers. The result exhibits the strengthening effect of the disulfide cross-links [58].

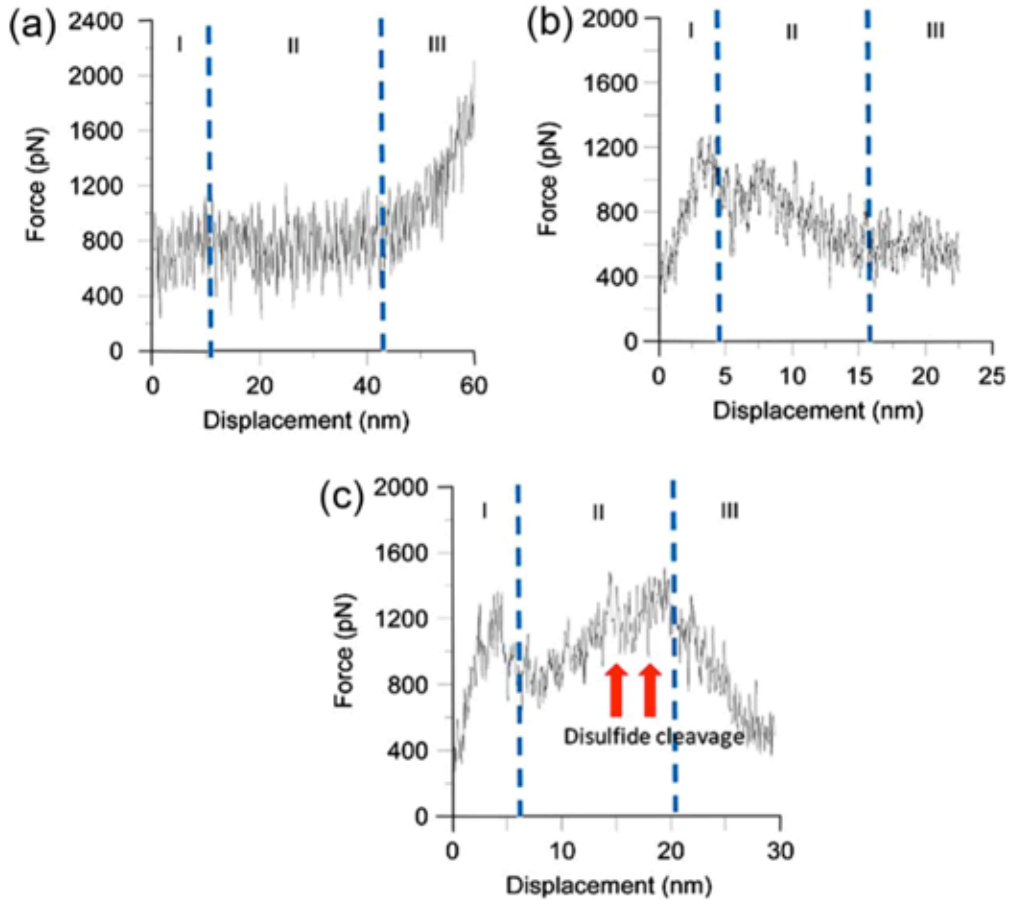

Figure 9. Atomic simulation of the tensile force-displacement curves for **(a)** heterodimer, **(b)** tetramer without disulfide cross-links and **(c)** tetramer with disulfide cross-links. Taken from [58].

Keratinous materials exhibit viscoelastic behavior, which is the combination of elastic and viscous components [59]. This viscoelastic behavior provides mechanical support and impact resistance for keratinous materials and is also related to energy absorption [59]. The viscoelasticity increases the strain rate sensitivity, which indicates a possible transition from ductile to brittle behavior with increasing of strain rate [59]. The energy absorption of horns and hooves is expected to have a profound relationship with

viscoelasticity. Viscoelasticity will attenuate elastic waves generated by impact on the horns from fighting and on the hooves from galloping [60].

2.2 Impact Resistant Natural Materials

Biological materials such as bones, teeth and tusks, hooves and horns are all energy absorbent natural materials. These materials are strong but lightweight, and they are capable of absorbing impact shock and sustaining repeated compressive loading. These structural biological materials are mainly composed of biopolymers (structural proteins such as keratin and collagen) with or without a mineral phase (calcium carbonate, carbonated hydroxyapatite or silica) [40]. Their hierarchical structure enhances the impact resistant ability. Table 4 lists several structural biological materials with the biological purpose, chemical composition, hierarchical structure and mechanical properties.

Table 4. Chemical composition, hierarchical structure, mechanical properties of several structural biological materials and their biological functions of some natural materials.

Material	Chemical composition	Hierarchical structure	Mechanical properties	Biological functions
Bone	Collagen fibrils: tropocollagen molecule (a triple helix of the collagen molecule) Mineral phase: calcium phosphate Water content: 15-25 vol.% [61]	Cancellous (trabecular or spongy) bone has a porous, lamellar structure, composed of platelets and rods. Cancellous bone is surrounded by compact bone [40]. Compact bone is composed of osteons, which have concentric lamellae with alternating oriented collagen fibrils dispersed inside and the lamellae surround a main vascular channel.	Cancellous bone resists high impact loads and ensure a flexural strength-to-weight ratio. It also provides spaces for bone marrow and vessels [40]. Compact bone is stiff but brittle, with a high Young's modulus of ~20 GPa but low strain to failure. The energy absorbing ability is low compared to keratinous materials [62].	Sustain large compressive stress and resist fracture.
Tooth and tusk	Outer: enamel layer: 92 vol.% hydroxyapatite, 2 vol.% collagen, 6 vol.% water. Core (dentin): 50 vol.% mineral, 30 vol.% collagen and other proteins, 20 vol.% water [63].	In the enamel a woven structure presents. The tubule density increases in the enamel region (4900 mm^{-2}) to the interior region (57000 mm^{-2}) [64]. In dentin, the mineral phase surrounds tubules, which generate perpendicularly to the pulp. Tubules are filled with fluid.	Enamel has a high hardness of 1.5 GPa and an elastic modulus of 80 GPa [63].	Tearing, gnawing, fighting, slicing, biting [40].
Hoof	α-keratin	Keratin cells organize into ~250 μm diameter tubules along the hoof length. The tubule is a hollow cavity of ~50 μm. Intertubular materials form angles to the tubule direction [65].	The maximum fracture toughness is 22.8 KJ/m^2, which is an order of magnitude higher than fresh bone. Hydration has an influence on its mechanical properties.	Absorb forces generated with the ground and transfer it to skeleton [46].
Horn	α-keratin	IFs are embedded in an amorphous matrix that forms a single keratin cell. Longitudinally aligned keratin cells form lamella and the lamellae are layered along the radial direction, with tubules dispersed between the lamellae. Tubules have a elliptical shape.	Horns are significantly tough, resilient and highly resistant to impact forces [46]. Mechanical properties are highly depended on humidity. The stiffness and strength has a gradient along the length of horn sheath.	A weapon to protect from predators, a shield to catch blows, a weapon to fight with other males to win mating privilege [23].

The structural biological materials listed in Table 1 have many structural similarities. Multiple, distinct reinforcing lamellae are found in bone, tooth, hoof and horn, all of which have unique deformation mechanisms to absorb energy. The lamella is assembled by strong and tough protein fibers (collagen or keratin) that are reinforced by minerals (bone, teeth) or are non-mineralized (hoof and horn). Tubules are a common structure in these materials. In bone, the tubules are present as vascular channels that are surrounded by concentric layers of a collagen/hydroxyapatite composite (osteons). In teeth, the tubules are surrounded by a highly mineralized collagen/hydroxyapatite peritubular layer. In hooves and horns, the tubules are long and extend along growth direction, surrounded by the keratin lamella. These hierarchical structures provide high energy absorption capability. Deformation mechanisms such as delamination and microbuckling of the lamellae can provide energy absorption without material fracture. In bone and teeth, an increase of mineral content increases strength but decreases the work of fracture. There is a tradeoff between toughness and strength. The horn has the highest work of fracture value with a zero content of minerals, while enamel has a nearly zero work of fracture with the highest mineralization. Also, enamel has the highest strength while the horn processes the lowest [40]. The diameter and density of the tubules also have an influence on the mechanical properties. The tubules can provide toughening mechanisms by squeezing closed, preventing extended regions of microbuckling and also deflecting cracks [40]. Hydration and location also play an important role in affecting mechanical properties [23]. With the increase of water content, stiffness decreases while toughness increases.

2.3 Horn Structure and Mechanical Behavior

Horns are used as a weapon to defend themselves or for combat with other males for mating rights, as a shield to catch blows, and possibly as an apparatus to regulate body temperature [23, 66]. The majority of horns are a lifelong appendage and cannot grow back once broken, therefore they should be tough, resilient and resistant to fracture [17, 67]. The morphology and hierarchical structure of a bighorn sheep horn is shown in Figure 10 [17]. Figure 10 (a) shows the morphology of the horn it grows in a spiral fashion with ridges on the surface due to seasonal growth spurts. It has a hollow interior, which at the base is filled with a porous bone. Three orthogonal directions are defined: the longitudinal direction is parallel to the tubule direction (growth direction), the radial direction is the impact direction and the transverse direction is perpendicular to both the longitudinal and radial directions. Figure 10 (b) shows the microstructure of the horn along transverse section. It has a three-dimensional laminated structure with tubules interspersed between lamella. The tubules are elliptically shaped with a major axis of ~100 μm and a minor axis of ~40 μm. The complete hierarchical structure is shown in Figure 10 (c) and (d). At the lowest level, the α-keratin helices assemble to form the IFs. The IFs are embedded in an amorphous matrix forming a single keratin cell. The keratin cell has a disk morphology with a large radius-to-thickness ratio. Keratin cells attach each other with their edges forming a single lamella with a thickness of 2-5 μm. These thin lamellae are layered along radial direction with their large faces attaching each other, forming a lamellar structure with tubules interspersed between the lamellae. The tubule density in the bighorn sheep

hors has a gradient along the radial direction from 8% ~ 12% at the outer surface to 0% at the inner surface [17].

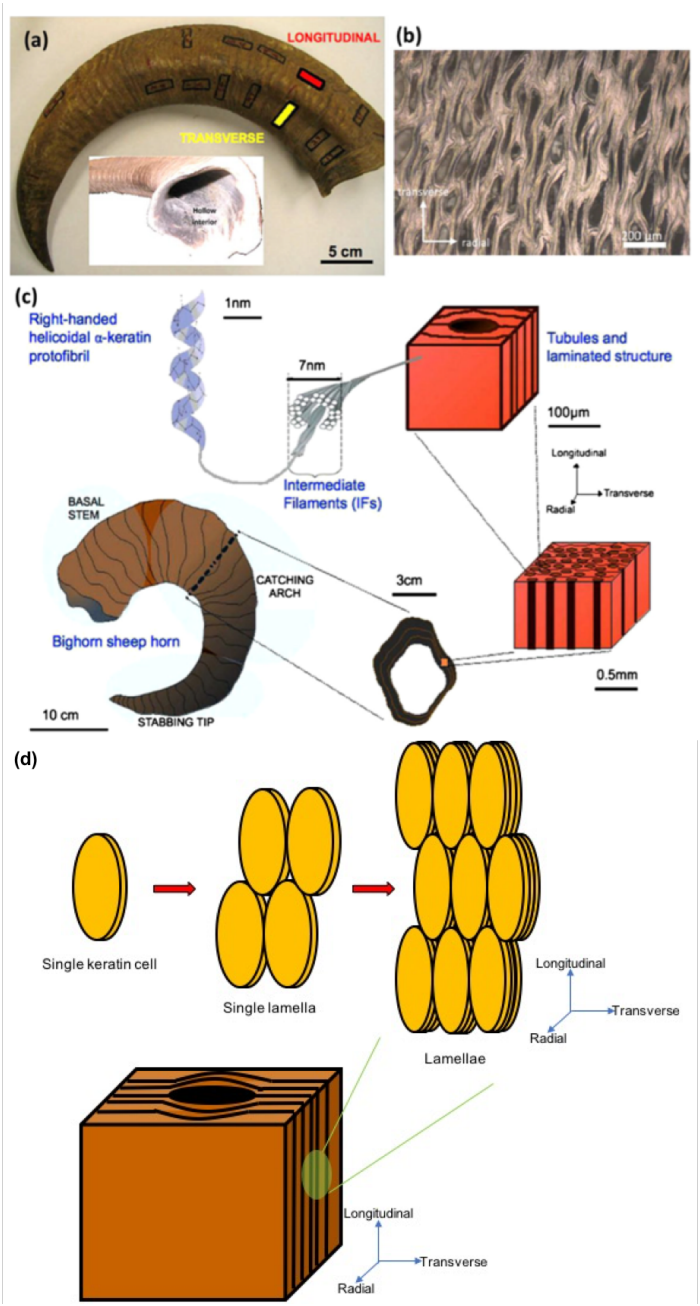

Figure 10. (a) Photograph of the bighorn sheep horn showing the spiral shape, ridges and the hollow interior; **(b)** microstructure of the horn (perpendicular to growth direction) showing laminated structure with tubules interspersed; **(c)** hierarchical structure of the horn. **(d)** schematic diagram of single keratin cell and cell arrangement. Adapted from [17].

The mechanical properties of various horns have been examined in the past. Experiments revealed that along the length of fresh waterbuck horns, the work of fracture (the area under the stress-strain curve of a pre-notched sample in three-point bending test) ranged from 10 to 80 kJ/m^2 [51]. Taking into account the specific gravity of different materials, the specific work of fracture of the horn is 32 kJ/m^2, which is greater than most other biological and synthetic materials (antler 6.6 kJ/m^2, bovine femur 1.6 kJ/m^2, glass 5 kJ/m^2, mild steel > 26 kJ/m^2) [68, 69]. Three-point bending tests of the cattle horn shows the mechanical properties are position dependent, shown in Figure 11. From the distal to the proximal region of the horn, the stiffness and strength decrease. This is likely due to the age of the horn. The distal region is the oldest while the proximal region is the youngest. This may help with the fighting behavior. During fights, the distal part needs to be hard enough to stab the opponent, whereas the proximal part should be tough to absorb energy. The gradient of mechanical properties is also due to water content and keratinization degree [70]. For the bighorn sheep, the gradient of porosity along growth direction would also alter the strength [17].

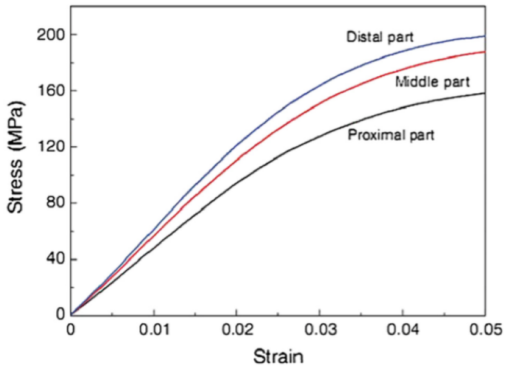

Figure 11. Three points bending stress-strain curves of samples obtained from different parts along the cattle horn. Taken from [70].

The mechanical properties are also highly dependent on water content. The Young's modulus and tensile strength decrease when hydration increases. The tensile strain-stress curves of cattle horn under different hydration level show highly hydration dependence, shown in Figure 12. When the water content increases, both Young's modulus and strength decrease [70] but the fracture strain increases. This dependence also applies to sheep horn [71] and oryx horn [72]. The hydration reliance of horns can be explained by water-matrix interaction, which was described in Section 2.1.2.

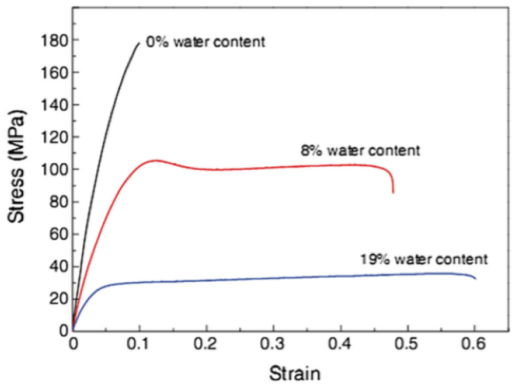

Figure 12. Stress-strain curves of cattle horn under tensile test; three hydration levels of sample were tested. Taken from [70].

Figure 13 shows the fracture surface of a bighorn sheep horn after three-point bending test. The sample was fractured along transverse direction. Fibrous and lamellar structure of the horn can be seen on the left image. IF bundles appear as small fibers embedded in the lamella. Delamination together with fiber fracture is evident. It appears that from the work of Kitchener on horns from gemsbok (*Oryx g.gazella*) [73] and Tombolato from horns from the bighorn sheep [17], horns have a delamination toughening mechanism and fiber bridging to further enhances the fracture resistance.

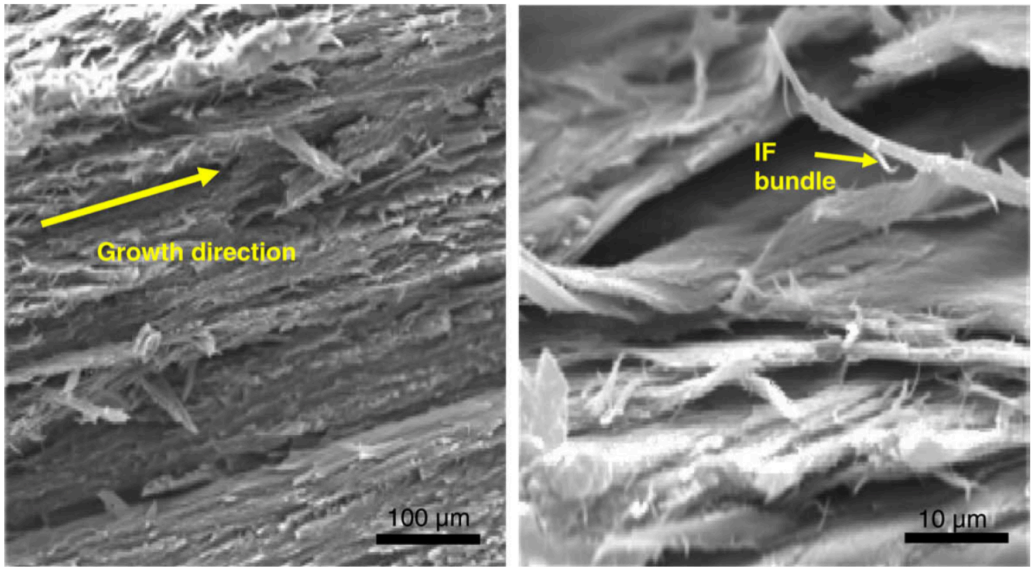

Figure 13. Scanning electron micrographs of the fracture surface of ambient dry bighorn sheep horn after three-point bending test. The sample was fractured in the transverse direction. Fibrous and lamellar structures are shown on the left; delamination and fiber breakage are shown on the right. Taken from [17].

2.4 Fighting Behavior

Each species has its unique fighting style. Horns should evolve specific structure to accommodation their fighting behavior. Figure 14 (a) shows the fighting behavior and external horn morphology of bighorn sheep. During clashes, the horns are used in a combination of karate chop, sledgehammer and shield [74]. The ram that attacks another ram will focus the impact on the combat edge of one horn, as shown in the figure, and clash into the other ram, while the defending ram will use its two horns to catch the attacking horn and dissipate the force. The force generated in clash is tremendous and can even cause shattering of the skull [74].

Figure 14 (b) shows the fighting behavior and external horn morphology of the domestic sheep. This horn is curlier than the bighorn sheep. It also has ridges on the surface due to seasonal growth spurts. The domestic sheep has a similar fighting behavior as the bighorn sheep but the opponents stand closer to each other and the clash has a lower speed than bighorn sheep. In both two species, the impact direction is along radial direction of the horn [75].

The mountain goat uses a different fighting style, which is stabbing, shown in Figure 14 (c). The opponents whirl in anti-parallel position of each other at the beginning, and then stab the opponents rear and belly using the tip of the horns. The fights between rams are rare and usually cause severe injuries [76]. This horn is short and straight, with an arc at the distal part. Growth ridges are only on the surface of proximal part. The central and distal parts of the horn are smooth.

There are two fighting modes engaged by the pronghorn. The first one is that two bucks suddenly clash together and the other one is that two bucks gradually approach each other and lower their head and then slowly engage their horns [77]. Fights involve thrusts and counterthrusts with the horns. When the horns are interlocked, the opponents use their body strength to twist the others neck and push him back to make the opponent lose balance. Figure 14 (d) shows engagement of two pronghorn horns. Unlike the other species, the horn is branched, and sheds and regrows every year. The horn has a sharp end and only becomes curved at around one-third from the distal point. It has two branches with one main branch growing from frontal to distal and a much smaller branch [77]. No ridges are observed on the surface of the horn.

Figure 14. Combat style and external horn morphology of four species: **(a)** bighorn sheep, **(b)** domestic sheep, **(c)** mountain goat and **(d)** pronghorn.

3 Hypotheses

Horns from the bighorn sheep, domestic sheep, mountain goat and pronghorn all have a short boney core and a longer keratin sheath surrounding the core. However, the microstructure and mechanical properties of these horns have not been fully investigated. This thesis aims to examine the microstructure and perform compression, tensile and impact teat of four horns and make comparisons. There are four hypotheses to be tested in this thesis:

(I) Keratinous horns should share similar microstructure but also have differences, given that two families are chosen and in one family, three species are represented.

(II) Difference in microstructure should affect the mechanical properties.

(III) Hydration has the influence on mechanical properties.

(IV) The microstructures and mechanical properties have been optimized to accommodate the various combat styles of each species.

4 Materials and Methods

Four pairs of bighorn sheep, domestic sheep, mountain goat and pronghorn horns were purchased from Wilderness Trading Company (Pinedale, WY). All horns were stored in air at room temperature.

4.1 Optical Microscopy

The microstructures were characterized by optical microscopy and scanning electron microscopy (SEM). A Leica Ultracut UCT Ultramicrotome (Leica Microsystems, Wetzlar, Germany) was used to get fine-polished ultra-thin horn slices (procedures are described in Appendix I). Samples were obtained from central region of the horn and in the middle from central line to surface along radial direction. Two samples of each horn were prepared with one cross-section parallel and one cross-section perpendicular to the longitudinal direction. The thickness of horn slices was 1 μm to 1.5 μm. Slices were stained by toluidine blue (a basic thiazine metachromatic dye with high affinity for acidic tissue components). Optical micrographs of stained horn slices were taken from a Zeiss AxioImager M1 optical microscope (Zeiss, Oberkochen, Germany).

4.2 Scanning Electron Microscopy (SEM)

Compressive deformation microstructures and tensile fracture surface morphology were obtained using scanning electron microscopy with an ultra-high resolution scanning electron microscope (FEI, Hillsboro, OR, USA) For compressive deformation characterization, surfaces were obtained from ambient dried and rehydrated samples

compressed along the longitudinal direction for a final deformation of 70%. A water-jet cutting machine was used to obtain the samples. Four sections were obtained from each compressed sample. The cutting position and loading direction are shown in Figure 15. Excess water was wiped off by water-absorbent paper tissues and sections were air-dried for 24 hours. For tensile fracture surface characterization, the fracture surfaces were directly examined. Samples were mounted on aluminum sample holders with fracture surfaces up. Surfaces were sputter-coated with iridium at 85 µA for 15 seconds by Emitech K575X Sputter Coater (Quorum Technologies Ltd, East Sussex, UK). Surfaces were then observed under the SEM in the secondary electron (SE) mode at 5 kV accelerating voltage.

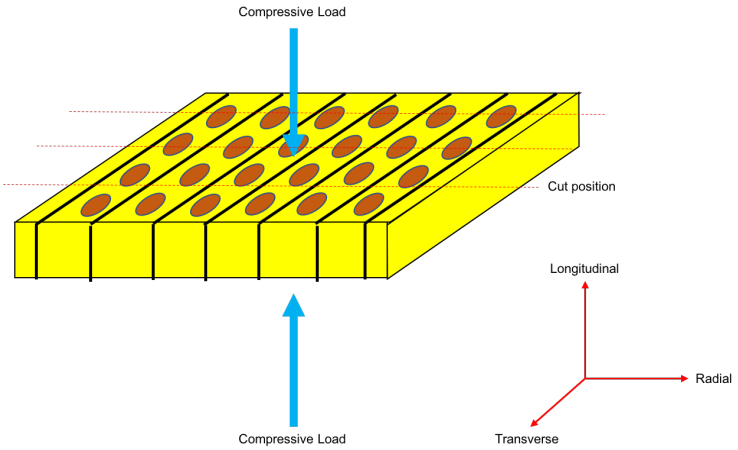

Figure 15. Compressed sample and the cutting position. Compressive load was applied in the longitudinal direction. After compression, samples were prepared by cutting samples parallel to the longitudinal direction.

4.3 Water Absorption Test

To investigate the water absorbing ability of different horn and evaluate the effects of moisture content, water absorption tests were performed. Two samples from each species were prepared. The samples had dimensions 6 mm × 6mm × 6mm. Samples were

air-dried for 24 hours before weighing. The samples were then soaked in purified water and weighed every 4 hours. The water was changed every 24 hours. After 126 hours, samples were taken out and the surface water was removed. The samples were then placed into pre-heated oven for 5 days to fully dehydrate. The temperature of oven was kept as constant at 60˚C. During dehydration, the samples were weighed every 12 hours.

4.4 Porosity Measurement

The porosity measurements were based on optical microscopy images of ultra-thin slices images taken perpendicular to the longitudinal direction. The software used to identify and measure the pores was ImageJ (a public domain, Java-based image processing program developed at the National Institute of Health, Bethesda, MD).

4.5 Compression Test

The three orthogonal orientations describing horns are longitudinal, radial and transverse. The longitudinal direction is parallel to the growth direction (proximal distal). The radial direction is perpendicular to growth direction and points from central line to surface (medial lateral). The transverse direction is perpendicular to both radial and longitudinal directions [17]. The three directions are shown in Figure 16.

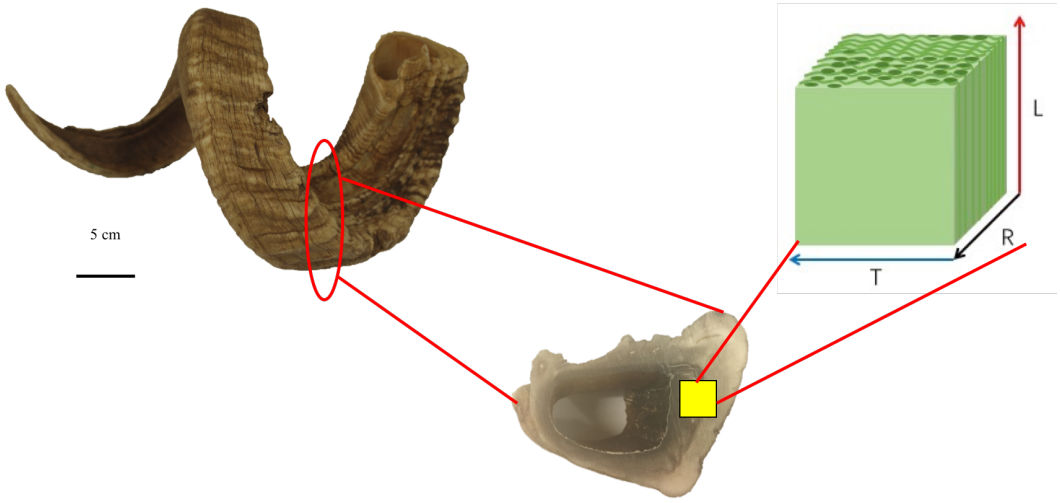

Figure 16. Three orthogonal orientations defining the horns. Longitudinal direction is parallel to grow direction (proximal distal), radial direction is perpendicular to growth direction and from central line to surface, and transverse direction is perpendicular to both longitudinal and radial directions. All compressive test samples were cut from the central region.

Cubic samples with dimensions of 6 mm × 6mm × 6mm were prepared. A section saw with circular diamond blade was used to cut the samples to obtain the most parallel surfaces. All samples were cut from the central region of the horn (shown in Figure 16). For each species, three sets of samples were prepared with the loading direction along longitudinal, radial and transverse directions. For each species, a total of 30 samples were prepared. Within these samples, 15 were tested in ambient dried condition and the others in fully rehydrated condition. For each condition, five each were tested in longitudinal, radial and transverse directions. The rehydrated samples were pre-soaked in purified water four days before testing [51] with the water changed daily and kept wet until testing. Compression test experiments were conducted on a universal testing machine equipped with a 50 kN load cell (EM Model 5869, Instron, MA, USA). The testing crosshead speed was controlled at 6 x 10^{-4} mm/s, which corresponds to a 1×10^{-4} /s strain rate. The machine

automatically stopped when strain reached 0.7. The stress (MPa) and strain (mm/mm) data were converted from the load-displacement data, obtained from software embedded in machine and stress-strain curves were drawn by OriginLab 2017 (OriginLab Corporation, Northampton, Massachusetts, USA) based on the raw data.

4.6 Tensile Test

Samples for tensile tests were cut from the central region of the horns. Rectangular samples with dimensions of 15 mm × 3 mm × 0.3 mm (length × width × thickness) were prepared using a water-jet cutting machine. Care was taken to cut the samples such that tubules were aligned parallel to the longitudinal direction [23]. Then the two ends of the samples were attached to 800 grit sandpapers to make dog-bone shaped samples. These samples had a gage length of 10 mm. For each species, a total of seven samples were prepared. The samples were kept under ambient conditions for one day until testing.

Tests were conducted on a universal testing machine equipped with a 30 kN load cell (Instron 3367 Dual Column Testing Systems, Instron, MA, USA). The crosshead speed was controlled at 0.001 mm/s, which corresponds to a 1×10^{-4}/s strain rate, same as in the compression tests. The machine was stopped manually when sample fractured. Load-displacement data from the machine were converted to stress-strain data by OriginLab 2017.

4.7 Impact Test

The ASTM standard D7136/D7136 M-07 [78] is applied for drop weight impact test of layered multidirectional polymer composite matrix, and the standard requires the test machine having a rectangular free-standing (unclamped) area with the dimension of 125 mm × 75 mm (length × width). Since it is difficult to get such large testing samples from the horns, a modification of the standard apparatus was applied. A lab built drop weight test machine built by Lee et. al. [22] (Figure 17) was used with a 1:5 scale of the ASTM standard test machine. The tip of the impactor has a hemisphere shape with a diameter of 3.2 mm. The freestanding area has a circular shape with a diameter of 12.69 mm, which is accomplished by drilling a circular hole in the center of the upper clamp. The drop weight is fixed at 1.2 kg and drop height varied from 0 to 0.74 m. Relating the potential to kinetic energy, the following equations were used:

$$v = gt \tag{1}$$

$$\frac{1}{2}mv = mgh \tag{2}$$

$$E = mgh \tag{3}$$

where E is the impact energy, h is the drop height, g is the gravitational acceleration, and t is the drop time. Since the maximum drop height is 0.74 m, the maximum drop velocity is 3.81 m/s. With a fixed drop weight, the maximum impact energy is 8.70 J.

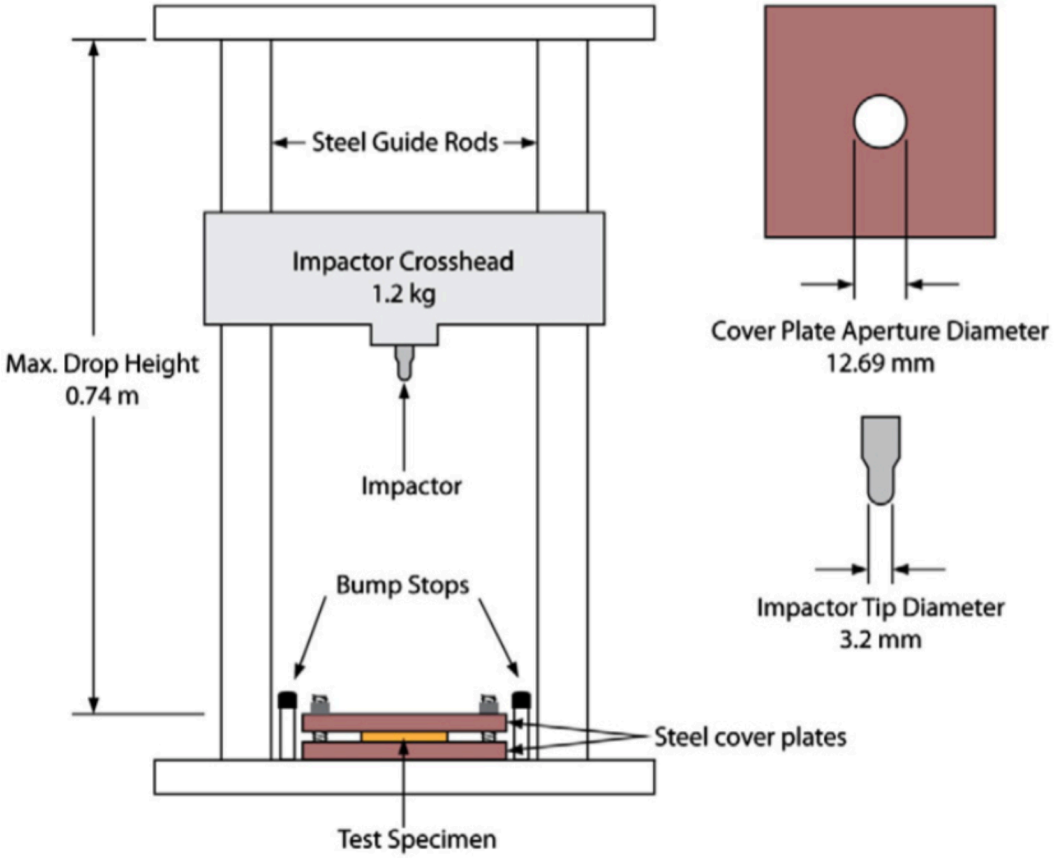

Figure 17. Schematic diagram of the modified impact test machine, showing the sizes of each component, taken from [22].

With a preset round free-standing area (a diameter of 12.69 mm), for this apparatus the optimal test sample dimensions to be clamped firmly are 20 mm × 20 mm (length x width). The bighorn sheep and domestic sheep have a cross-sectional diameter of horn ~70 mm and a thickness of keratin sheath of an average ~12 mm, so the diameter-to-thickness ratio is 5.83. Given consideration of best simulating natural dimensions of the horn and the ability to obtain adequate testing samples, the optimal thickness of the bighorn and domestic sheep samples is around 3.5 mm, which correlated to a length-to-thickness ratio of 5.72, close to the real ratio. For pronghorn, the average cross-sectional diameter of horn is ~40 mm and the average thickness of keratin sheath is ~6.5 mm, which corresponds to a

thickness of testing samples of 3.25 mm. But given the oval shape and the very rough surface of the horn, as well as the limited thickness of keratin sheath, adequate samples (an amount more than 35) were extremely hard to obtain. For mountain goat, the size of the horn is much smaller than the others (a length of 20 cm and a maximum diameter of 4.5 cm). Due to the existing of bony core, at the proximal part of the horn, the thickness of keratin is < 2 mm. Given the circular shape of the horn, it is impossible to get the testing samples from that part without cutting into bony core. While at the distal part, the bony core disappears, but the diameter of the horn is less than 20 mm, which the length and width requirements of the sample cannot be met. Therefore, only samples from the bighorn and domestic sheep were prepared. Since these two species have similar clashing fight style and the impact stress is mostly in the radial direction of the horns, the most impact resistance direction is hypothesized to be in the radial direction. All samples were impacted parallel to radial direction to mimic their natural condition. Samples with dimensions of 20 mm × 20 mm × 3.5 mm (length × width × thickness) were prepared by hacksaw. A total of 44 samples of bighorn and 36 samples of domestic sheep were prepared. All samples were cut and kept in air at room temperature until testing.

The normalized impact energy was calculated based on the equation [22]:

$$E_n = \frac{E}{d_s T} \tag{4}$$

Here E_n is the impact energy normalized to specimen thickness, d_s is the diameter of free-standing area, T is the thickness of the specimen. The specimens of bighorn sheep

were sorted into eight groups and each group had the same normalized impact energy ranging from 20 kJ/m^2 to 80 kJ/m^2. The specimens of domestic sheep were divided into five groups with normalized impact energy ranging from 30 kJ/m^2 to 60 kJ/m^2.

5 Results and Discussion

5.1 Structural Characterization

Low magnification optical micrographs of ultra-thin horn slices cut perpendicular to longitudinal direction are shown in Figure 18. Figure 18 a-d are the transverse sections of the bighorn sheep, domestic sheep mountain goat and pronghorn, respectively. As exhibited in figures, the shape and size of the pores (cross-section of the tubules) vary among different species. Elliptically-shaped pores exist in bighorn sheep and pronghorn. For the bighorn sheep, pores are more evenly distributed and similar in size (70 μm x 35 μm). For the pronghorn, the pores tend to disperse stochastically between lamellae and have a wider range of size (from 28 μm x 10 μm to 97 μm x 37 μm). The pronghorn horn has several large pores (only one shown in the image), with a major and minor axis dimension of 152 μm and 121 μm. These large pores were not observed in the other three horns. Pores from the domestic sheep show a deformed oval shape with a large length to width ratio of 5.7 (a major axis dimension of 80 μm and a minor axis dimension of 14 μm). For the mountain goat, the tubules were not identified.

SEM micrographs of the fracture surface from pronghorn sample after fracture in LN_2 are shown in Figure 19. Hair-like fiber bundles fill this pore. When fractured, the fiber bundles appear to have pulled out, leaving behind a hollow pore. Another possibility is that the fiber bundles remain in the pore, but are far longer than the residual length of tubules. This may indicate a loose adhesion between fiber bundle and tubule inner surface. Another hypothesis is that fiber bundles are stronger than the matrix since fiber bundles are minimally fractured and more likely pulled out thorough the tubule. The porosity of

thehorns is given in Table 5. The bighorn sheep horn has the largest porosity of 11.3%. Domestic sheep and pronghorn have the second the third porosity of 7.7% and 5.8%. The mountain goat horn has nearly 0% porosity.

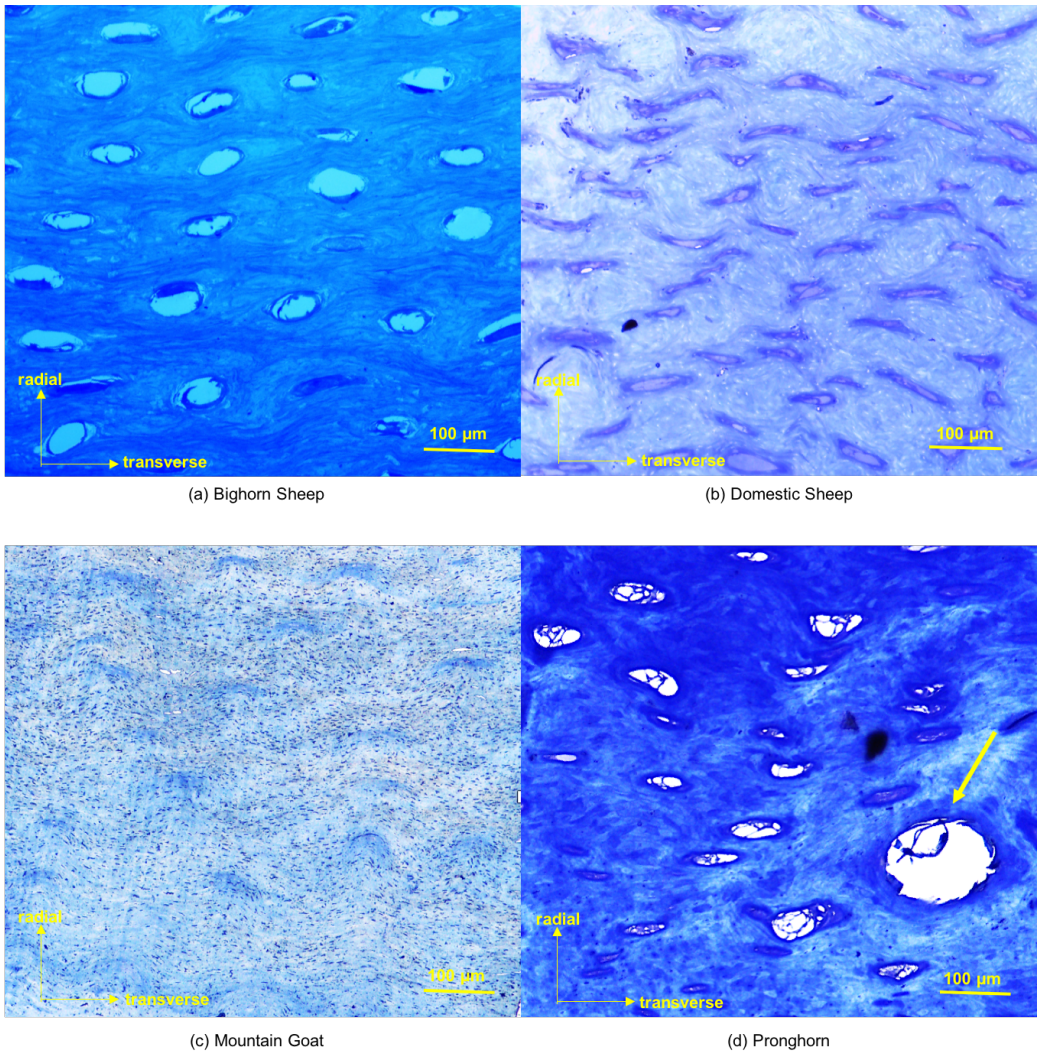

Figure 18. Low magnification optical micrographs of horn slices perpendicular to the longitudinal direction. **(a)** Bighorn sheep horn have elliptically shaped pores. **(b)** Pores of domestic sheep horn have a deformed oval shape. **(c)** Pores are hardly seen in mountain goat horn. **(d)** Pores in the pronghorn horn are of similar shape and size to those in the bighorn sheep. A large pore is also observed.

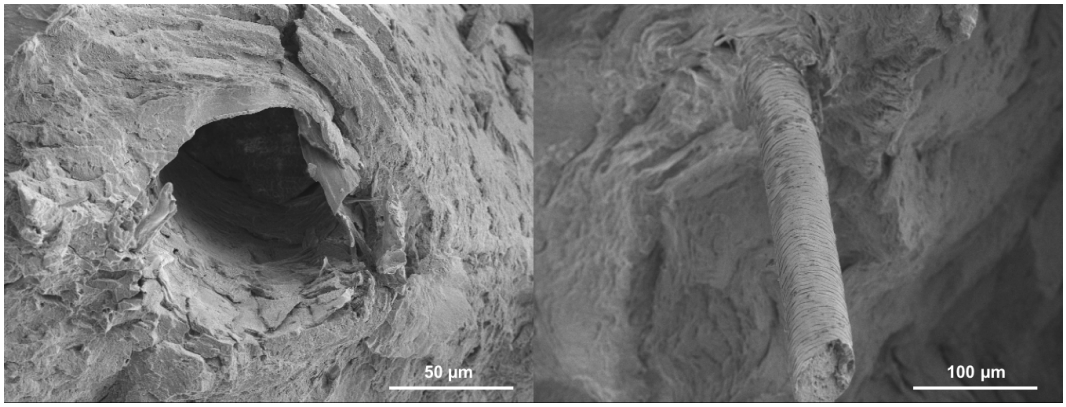

Figure 19. Fracture surface of pronghorn horn broken in LN_2. A tubule with fiber pulled out is shown in the left and hair like fiber bundle is shown in the right.

Table 5. Porosity and average pore size of the different horns.

Species	Bighorn sheep	Domestic sheep	Pronghorn	Mountain goat
Porosity (%)	11.3	7.7	5.8	~0
Average pore size (major axis × minor axis, µm)	70 × 35	80 × 14	72 × 23	Not found

Higher magnification optical micrographs of the transverse sections from different horns are shown in Figure 20. The lamellae layering manner can be seen from these images, showing a high similarity between the different horns. The lamellae layered in the radial direction with their faces attached each other and creating a wavy pattern surrounding the tubules (if the horn has tubules) [17], as illustrated in Figure 10 (d). This result indicates there is a common layering pattern of the lamellae in the different horns.

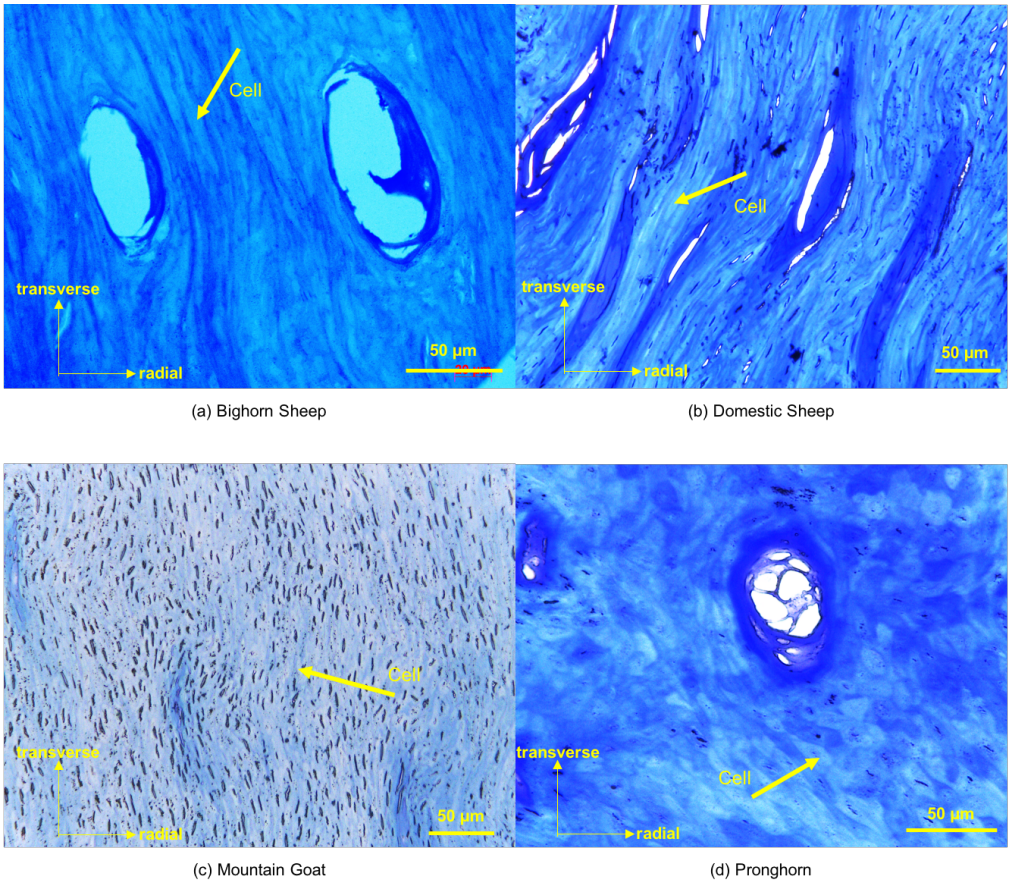

Figure 20. High magnification optical micrographs of horn slices perpendicular to the longitudinal direction. Keratin cells are shown for **(a)** bighorn sheep, **(b)** domestic sheep, **(c)** mountain goat and **(d)** pronghorn. The lamellae are layered in the radial direction and form a wavy patten around the tubules.

Micrographs of the longitudinal sections reveal the keratin cell morphology and relationship between keratin cell alignment and tubule growth direction (Figure 21 (a)-(d)). Keratin cells have a disk-shaped morphology [70], roughly spherical with the radius much larger than the thickness of the disk. In the longitudinal direction, the cells are attached edge-to-edge, forming a lamella, as shown in Figure 10 (d). For horns that have tubules, the tubules extend along longitudinal direction with no termination observed. However, diversities exist among the species. In the bighorn sheep (Figure 21 (a)), the parallel

lamellae form a 41˚ angle to the tubule direction. In the domestic sheep (Figure 21 (b)), the lamellae are layered in a more disorderedly manner than in other horns. The lamellae that are close to the tubules tend to be layered parallel to the tubules, whereas away from the tubules, the lamellae form an acute angle to the tubule growth direction. As shown in Figure 21 (c) and (d), in the mountain goat and pronghorn, the lamellae are layered parallel to each other and to the tubule direction.

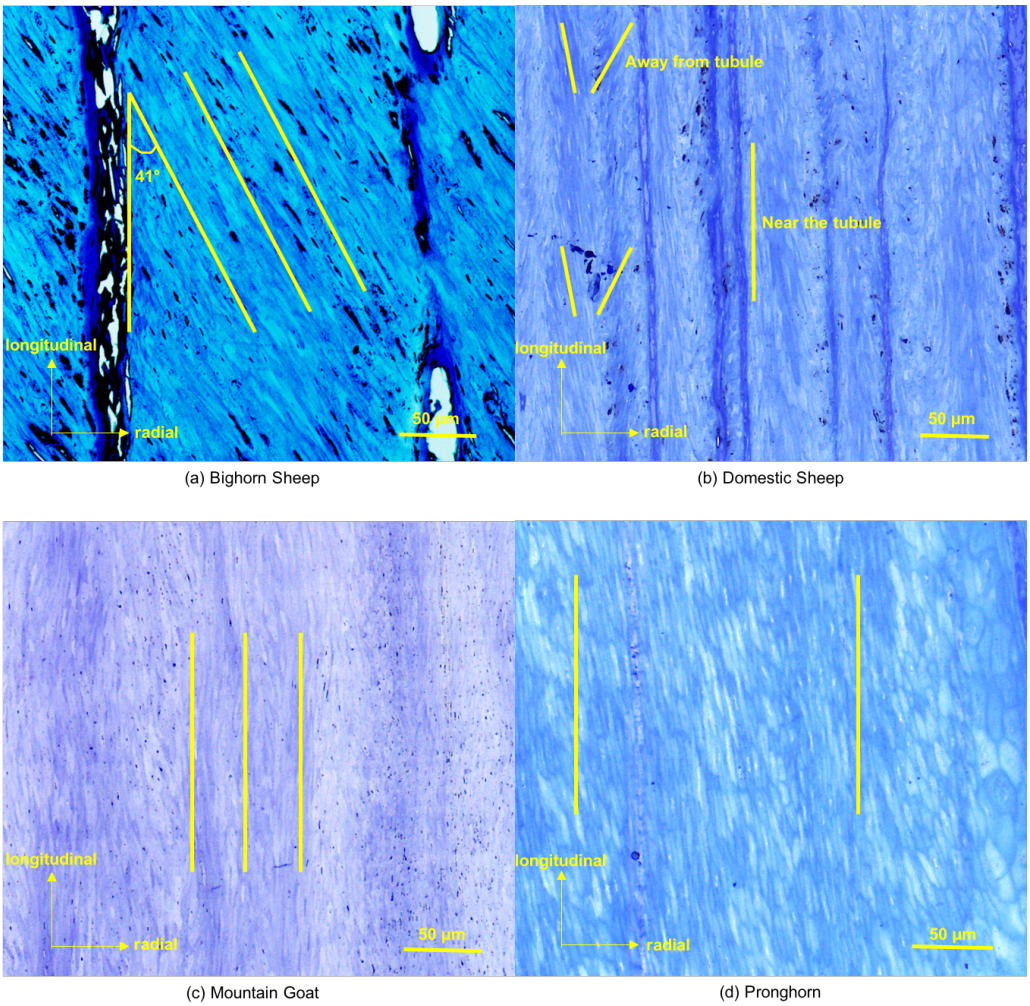

Figure 21. Optical micrographs of longitudinal sections of the horns. For all horns, the keratin cells have large length (cell diameter)-to-width (cell thickness) ratio. **(a)** Bighorn sheep lamellae form a 41° angle to tubule direction, **(b)** domestic sheep lamellae arrange more disorderedly, **(c)** mountain goat lamellae and **(d)** pronghorn lamellae are layered parallel to each other and to the tubule direction.

Higher magnification micrographs of the longitudinal cross-section are shown in Figure 22 (a)-(d). Slight differences between species can be observed. For the bighorn sheep (Figure 22 (a)) and domestic sheep (Figure 22 (b)), as for the morphology of single keratin cell, the cells are more irregular and tend to have sharp arcs and some protuberances. For the mountain goat (Figure 22 (c)) and pronghorn (Figure 22 (d)), the cells are more uniform and have a larger length to width ratio compared to the sheep.

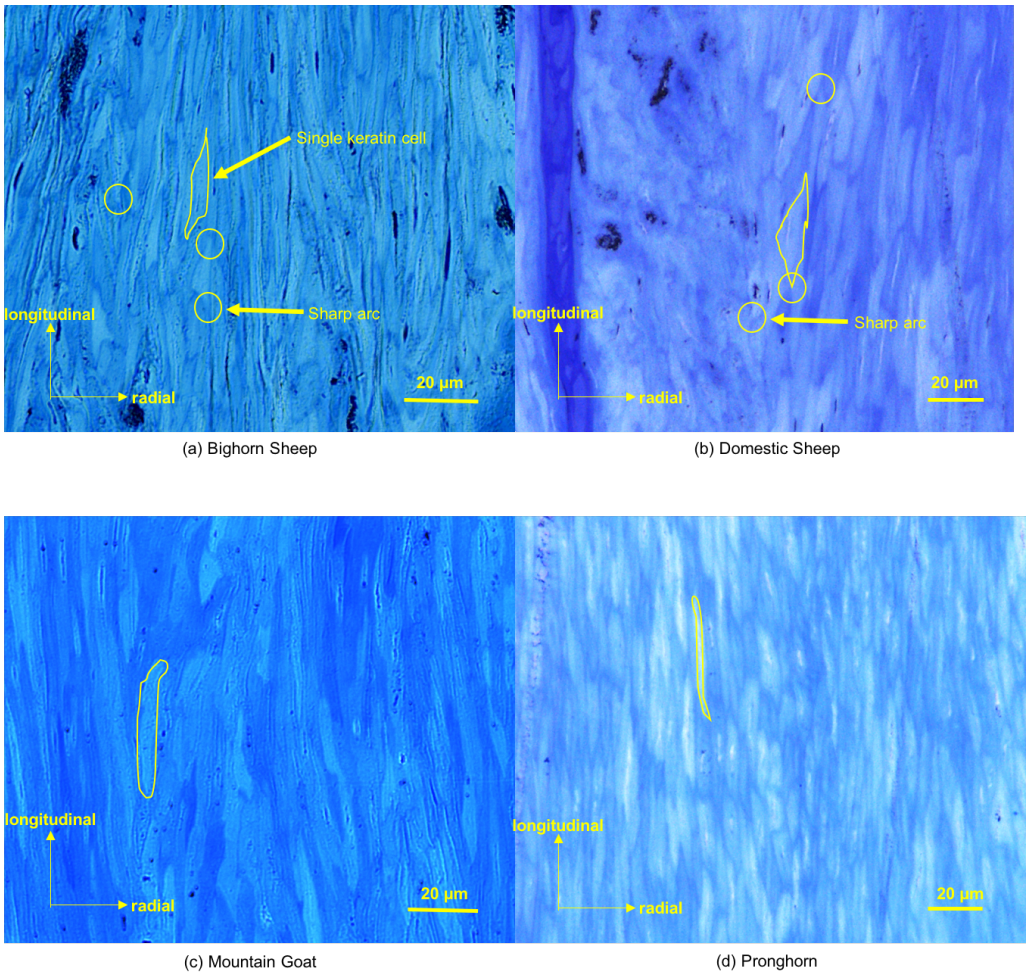

Figure 22. High magnification optical micrographs of the longitudinal sections. Keratin cells of **(a)** bighorn sheep and **(b)** domestic sheep turn to have more sharp arcs and protuberances. Cells of the **(c)** mountain goat and **(d)** pronghorn are thinner with a more regular oval shape.

Water absorption test results are shown in Figure 23. In the ambient condition, the water content of different species shows only slight differences, ranging from mountain goat (3 wt.%) to pronghorn (8 wt.%). After submersion in purified water for over 126 hours, the pronghorn shows the largest water absorption (44 wt.%). Figure 24 indicates that there are numerous nanopores inside the pronghorn cells, which is not found in other three species. Therefore, both tubules and the nanopores should be considered as a medium to hold water, since the water content of rehydrated samples from mountain goat, domestic and bighorn sheep is positively related to their porosity. Nanopores in the keratin cells also have an obvious effect on water content. Water can be stored in the nanopores; therefore, pronghorn horn absorbs significantly more water than other horns.

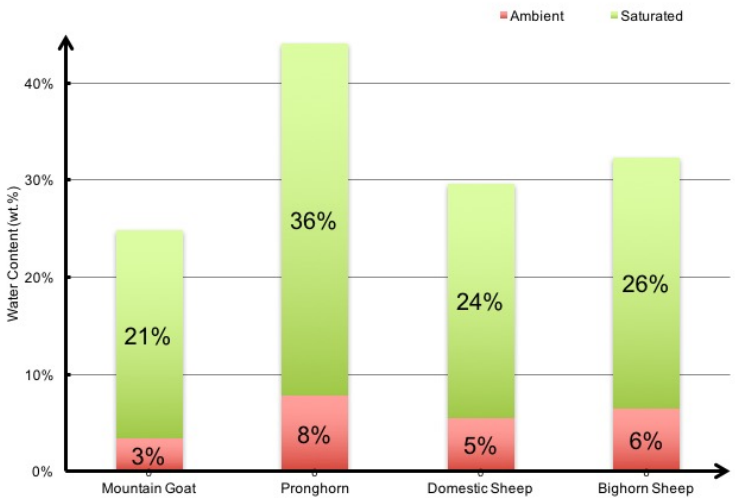

Figure 23. Water content (wt.%) of horns both in the ambient and fully rehydrated conditions. Water content of different horns is similar under ambient environment. When fully rehydrated, the pronghorn has a significantly larger water content than the other horns.

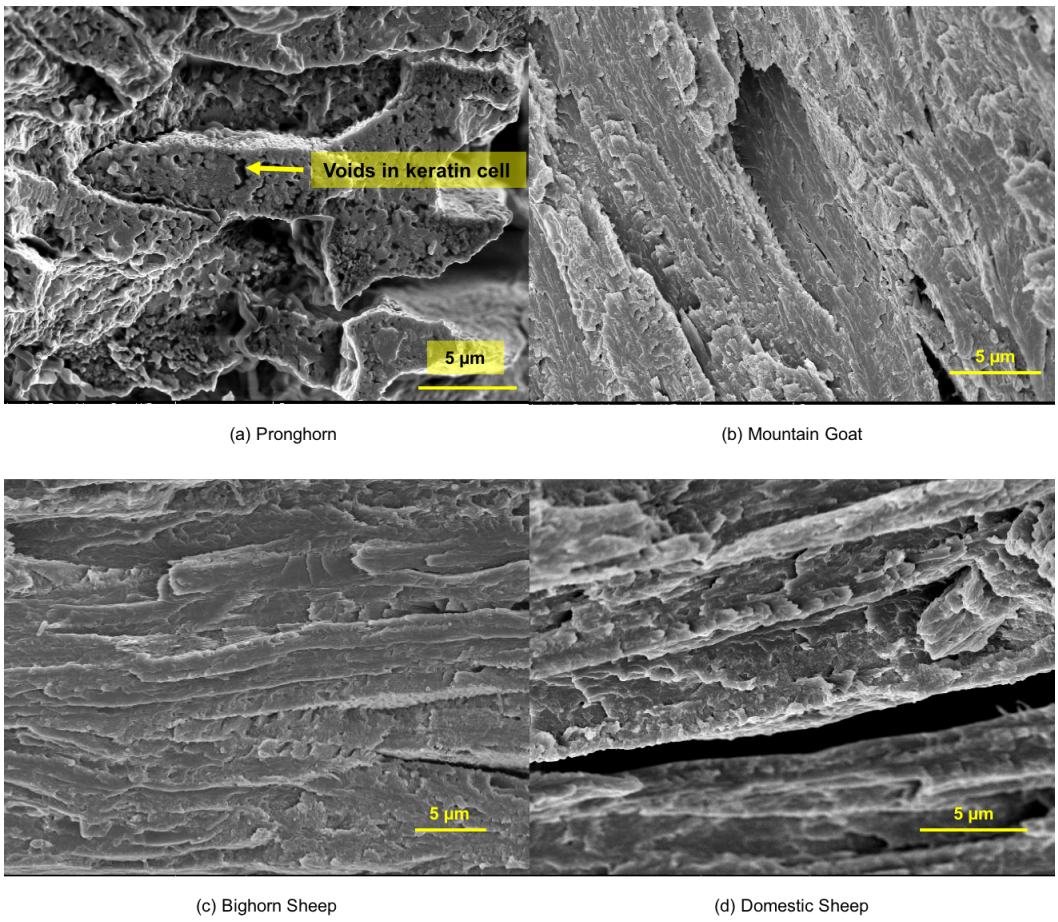

Figure 24. Scanning electron micrographs of the longitudinal cross-sections. **(a)** There are nanopores in pronghorn keratin cells. No obvious voids are observed in the cells of the **(b)** mountain goat, **(c)** bighorn sheep and **(d)** domestic sheep. Water can reside in these nanopores, therefore the pronghorn has a large water containing capability.

5.2 Mechanical Properties

5.2.1 Compression Test

The strain-stress curves of the ambient condition horns are shown in Figure 25. Strain-stress curves in all directions exhibit the same trend, which is a linear elastic deformation region followed by a long plastic region and ended with a crushing densification region. All horns present high strains with a deformation of ~70% without

failure. However, anisotropic behavior is evident when comparing the curves loaded in the longitudinal, radial and transverse directions. When compressed along longitudinal direction, shown in Figure 25 (a), the horns show a long plastic region with nearly constant stress. The tubules extend along longitudinal direction and when compressed, the tubules can delaminate and microbuckle, facilitating a large deformation. When compressed along other directions, where tubules extend perpendicular to loading direction, the tubules can more easily close and less space is provided for the lamellae to deform. Therefore, the compressive stress increases more rapidly, as shown in Figure 25 (b) and (c).

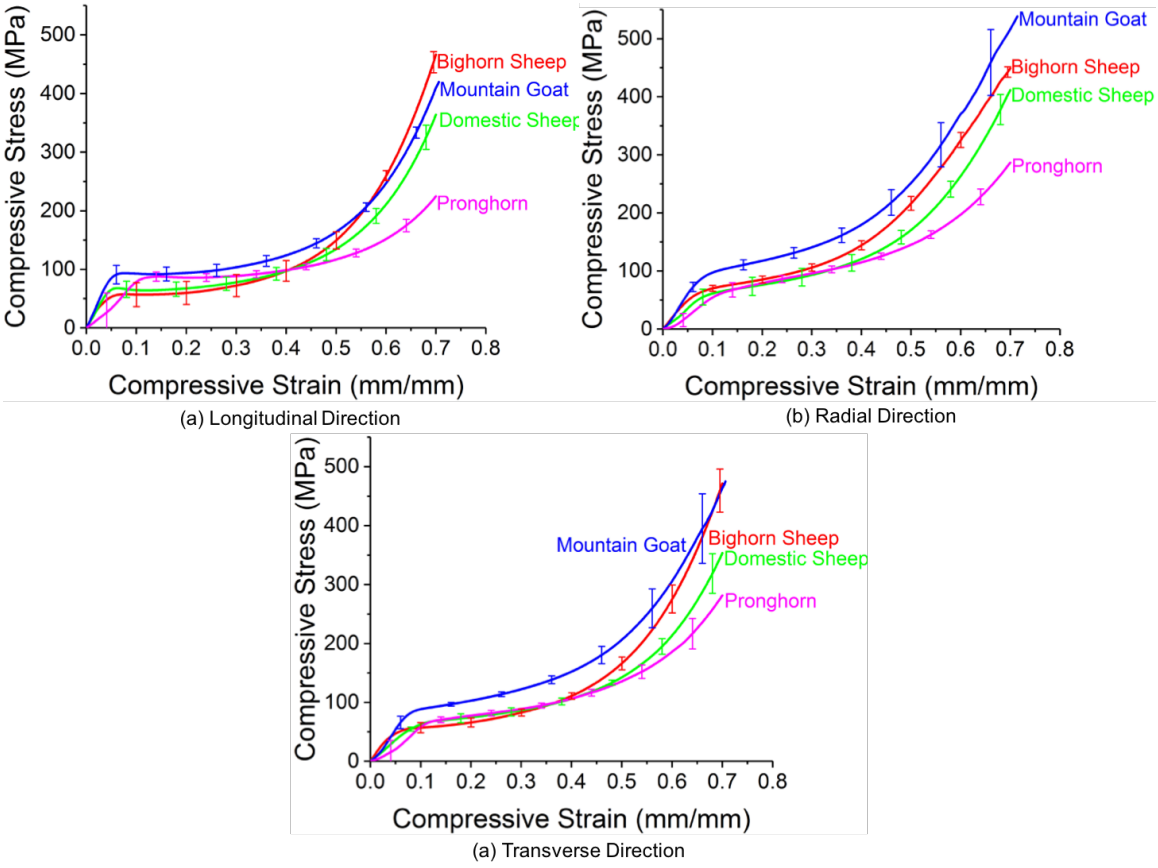

Figure 25. Compressive stress-strain curves comparison of different ambient dry horns in **(a)** longitudinal direction, **(b)** radial direction and **(c)** transverse direction. (n = 5)

The mechanical properties of ambient dry horns in compression tests are listed in Table 6. The yield strength is taken as the point on the strain-stress curve separating the elastic region and plastic region (where the slope of the curve begins to change). The resilience is calculated as the under area under the strain-stress curve up to the yield strength. The toughness is measured as the area under the strain-stress curve up to a strain of 70%. For all horns, the longitudinal direction has the highest Young's modulus and yield strength while the radial direction has the highest resilience and toughness. Since in the longitudinal direction the tubules are aligned parallel to loading direction, the tubules may strengthen the structure during elastic deformation. The lamellae also have their thin edges facing the longitudinal direction, which give more support to resist deformation. While in the radial direction the lamellae are stacked with their faces along the loading direction, which increase the difficulty to deform the lamellae, therefore the horn can be more resilient and tough along this direction. The yield strength of pronghorn and mountain goat is larger than bighorn and domestic sheep, which may correspond to their fighting styles. The fights of pronghorn and mountain goat involve stabbing and thrusting, and the high yield strength makes the horns strong enough to maintain structural integrity during the stabbing. The parallel layering of the lamellae in the longitudinal direction may contribute to a high yield strength.

Table 6. Young's modulus, yield strength, resilience and toughness of ambient dry horns in three directions.

Species	Pronghorn	Bighorn sheep	Domestic sheep	Mountain goat
Young's modulus (longitudinal direction, GPa)	1.8±0.2	1.7±0.5	2.0±0.2	2.1±0.6
Young's modulus (radial direction, GPa)	0.9±0.3	1.2±0.2	1.3±0.5	1.5±0.2
Young's modulus (transverse direction, GPa)	1.2±0.2	1.3±0.6	0.9±0.3	1.4±0.4
Yield strength (longitudinal direction, MPa)	85.5±6.4	67.8±7.9	64.3±13.5	81.6±22.2
Yield strength (radial direction, MPa)	67.5±4.2	57.3±5.3	63.1±8.9	82.3±9.8
Yield strength (transverse direction, MPa)	59.9±7.9	49.3±9.0	59.5±6.1	76.1±2.5
Resilience (longitudinal direction, MJ/m^3)	2.3±0.4	1.8±0.5	1.6±0.2	2.1±0.6
Resilience (radial direction, MJ/m^3)	2.4±0.5	2.0±0.4	2.5±0.9	2.8±0.7
Resilience (transverse direction, MJ/m^3)	1.9±0.5	1.3±0.5	2.6±0.6	2.4±0.3
Toughness (longitudinal direction, MJ/m^3)	72.5±2.5	92.1±9.5	83.5±5.1	103.4±5.8
Toughness (radial direction, MJ/m^3)	82.0±5.6	117.0±4.5	98.1±5.6	141.0±16.0
Toughness (transverse direction, MJ/m^3)	78.1±5.7	98.4±5.4	85.2±3.0	120.1±8.8

The deformation microstructures for each horn after 70% strain in the longitudinal direction were observed under SEM. After deformation, the samples were cut parallel to the tubule direction to examine more clearly the deformation inside the samples. Figure 26 shows the inner section of a deformed bighorn sheep horn. Figure 26 (a) shows a section near the side of the sample. Delamination around the tubules occurred, which generated a large crack. Figure 26 (b) shows the same cross-section taken towards the center. Similar to the sample edge, delamination is along the direction where maximum shear stress

generates, 45° to compressing direction [23]. A close up of a delaminated region is shown in Figure 26 (c) and fiber bridging is shown in Figure 26 (d). Fibers bridging between two lamellae appears to prevent further separation of the two detached lamellae.

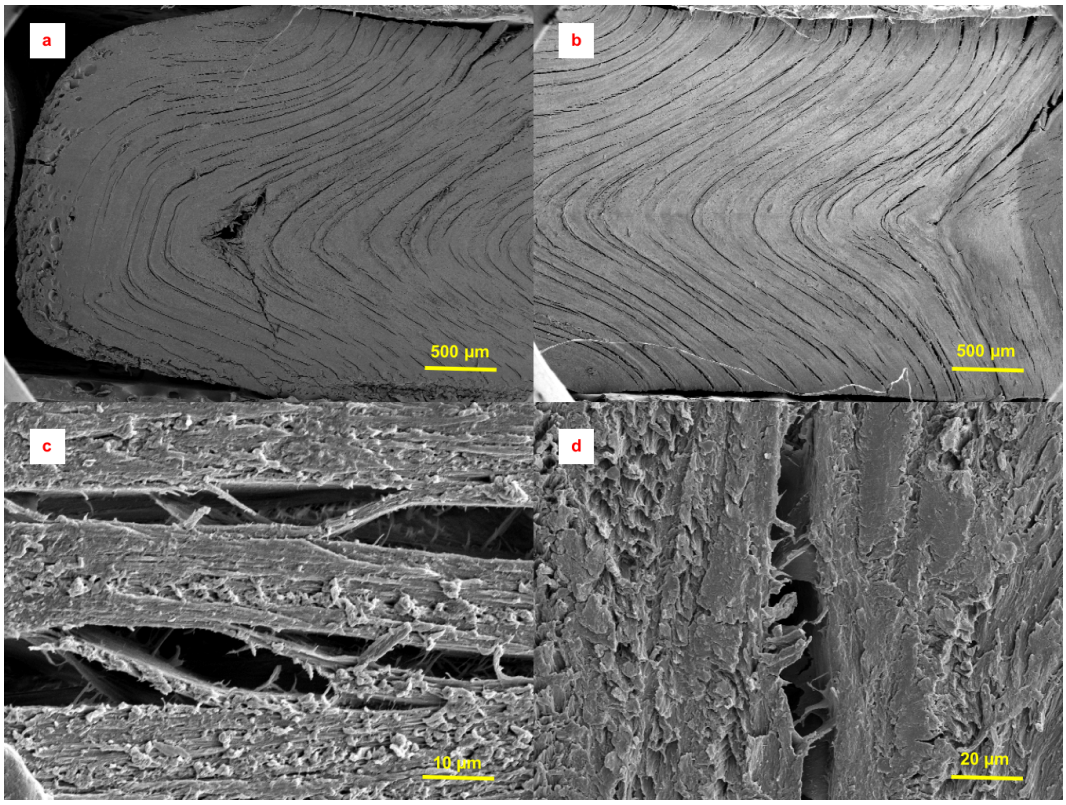

Figure 26. Scanning electron microscopy images showing inner sections of the bighorn sheep horn after 70% compression. **(a)** near the side surface of the sample and **(b)** near the mid-section of the sample. **(c)** Close up view of a delamination and **(d)** fiber bridging between two lamella are shown.

The domestic sheep shows similarity to the bighorn sheep, but there are some differences. An inner section of compressed sample from the domestic sheep is shown in Figure 27. Delaminated regions are observed near the top of the side surface and small, discontinuous cracks are observed near the bottom of the side surface (Figure 27 (a)). As opposed to the bighorn sheep, the extent of delamination is much reduced in the mid-section of the sample (Figure 27 (b)). Again, delamination is observed on the top and

small, discontinuous cracks are observed on the bottom of the middle surface (Figure 27 (b)). Two detached lamella are connected by fibers and similar to the bighorn sheep are shown in Figure 27 (c).

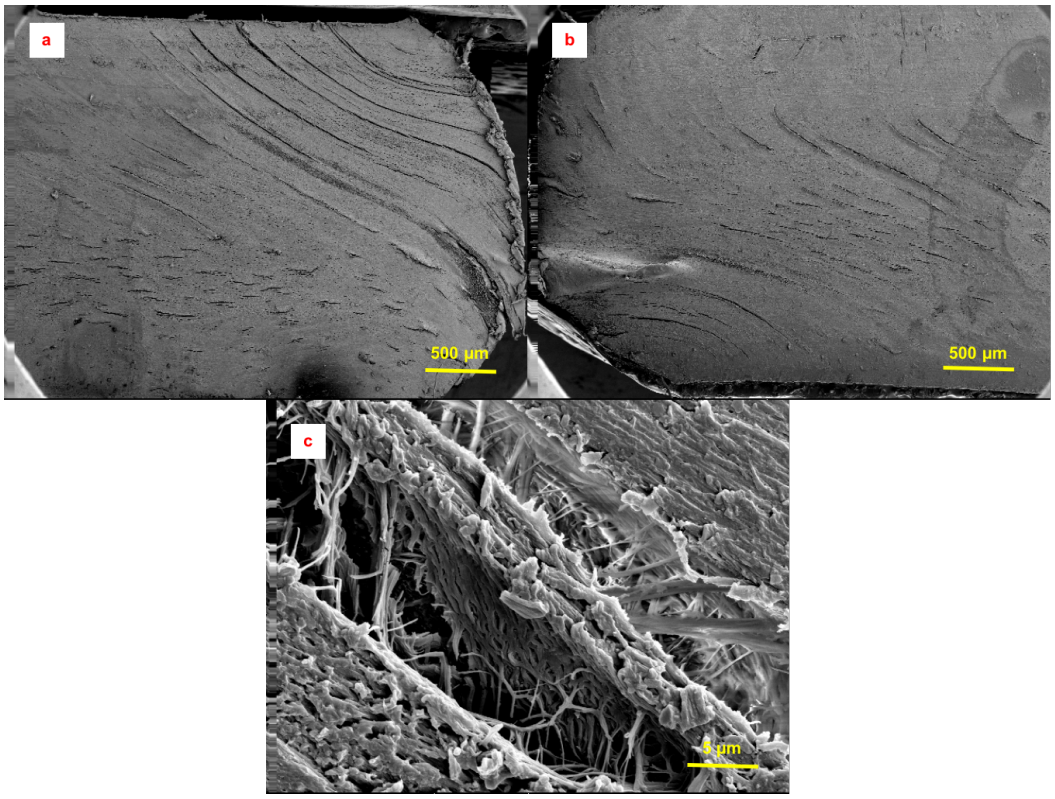

Figure 27. Scanning electron microscopy images showing inner sections of domestic sheep horn after 70% compression. **(a)** Image near the side surface of the specimen and **(b)** near the mid-section of the specimen. **(c)** Delamination and fiber bridging are shown.

For the mountain goat, extensive cracking is observed along with delamination near the side surface of the sample (Figure 28 (a)). In the mid-section (Figure 28 (b)), cracks are short and discontinuous, which are similar to the domestic sheep. Delamination and microbuckling are shown in Figure 28 (c). Fibers connecting two lamellae are thicker and longer than the other horns, which may be an aspect leading to the high compressive strength compared to the others.

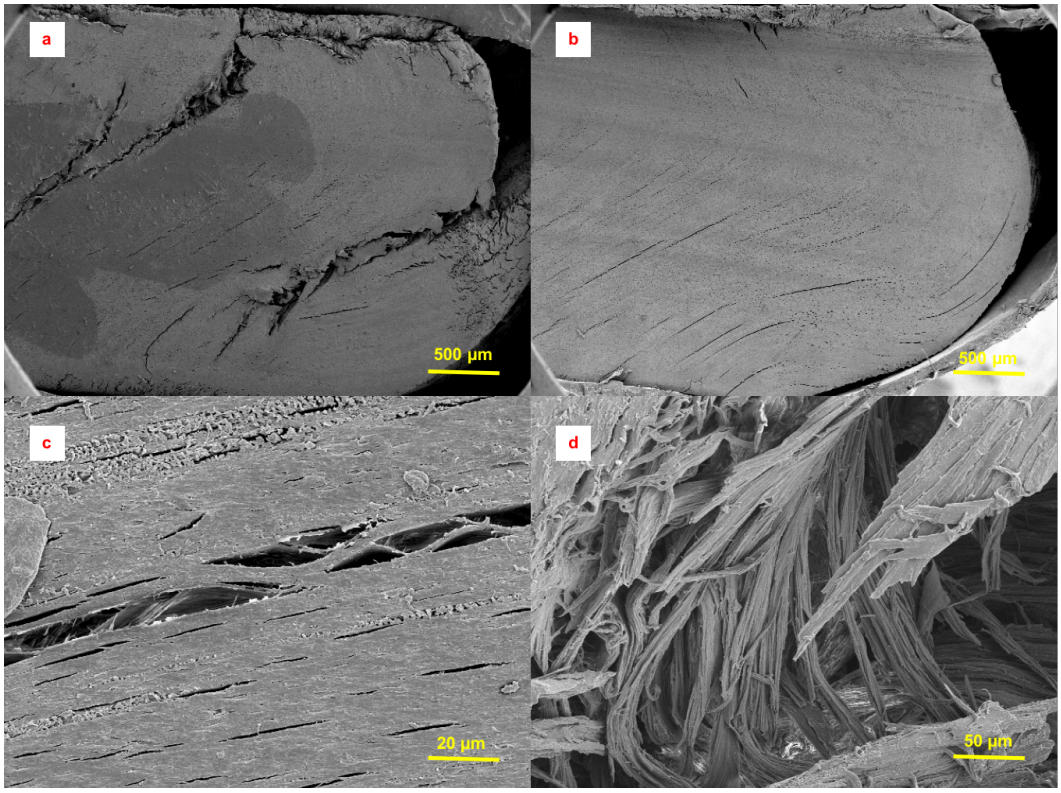

Figure 28. Scanning electron microscopy images showing inner sections of the mountain goat horn after 70% compression. **(a)** Large cracks are shown on the section near the side surface of the specimen, and **(b)** along the mid-section the cracks turn to be short and discontinuous. **(c)** Delamination and buckling is observed between lamella.. **(d)** Fiber bridging is more extensive than in the other horns.

Pronghorn micrographs are shown in Figure 29. On the inner section near the side surface of the specimen, shown in Figure 29 (a), delamination that is similar to the sheep horns is observed. In the mid-section (Figure 29 (b)), the direction and length of the delaminated region is very similar to the bighorn sheep, but the distance between delaminated regions is slightly larger. Microbuckling and fiber bridging are observed in Figure 29 (c).

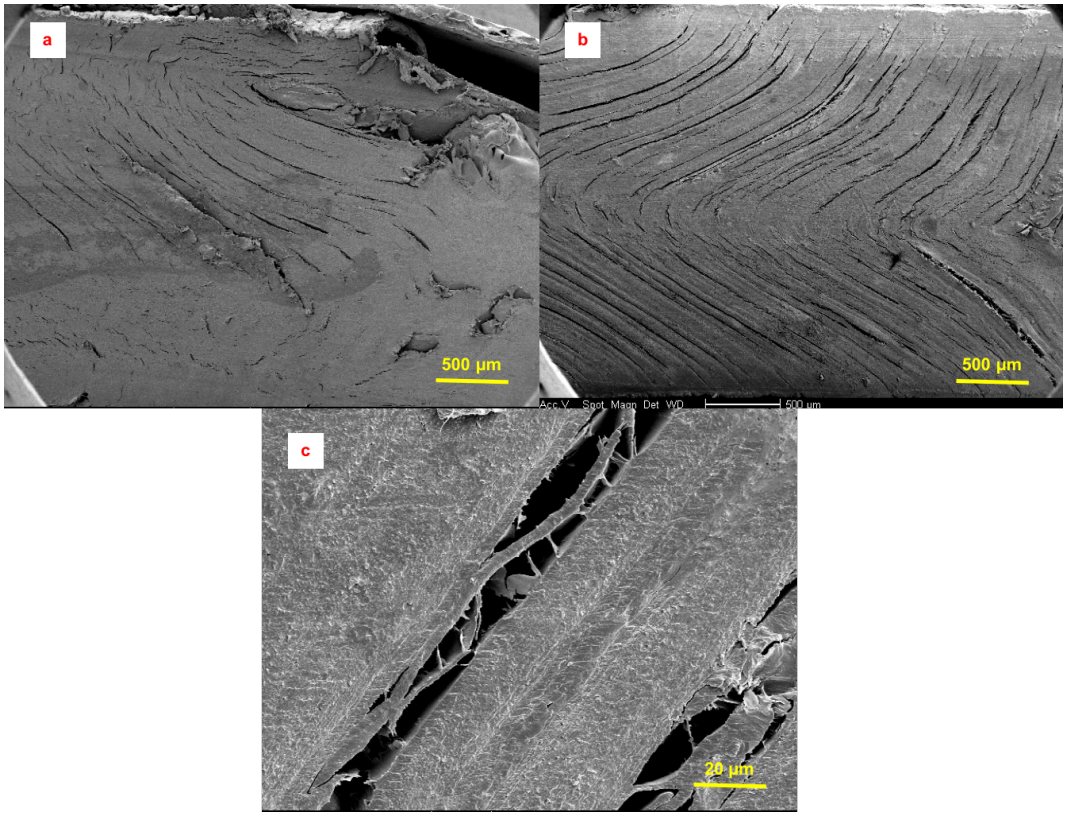

Figure 29. Scanning electron microscopy images showing inner sections of pronghorn horn after 70% compression. **(a)** Near the side surface of the specimen and **(b)** near the mid-section. **(c)** Delamination and fiber bridging are observed.

Comparing the four horns, the energy absorption mechanisms can be concluded. Delamination and microbuckling are the two main methods absorbing compressive stress. Fiber bridging restrains the separation of two detached lamella, preventing the generation of large cracks that may propagate to cause the failure. Due to this energy absorption mechanism, horns can deform 70% from its original size without failing. When species fight with each other, the large energy absorption prevents not only the horns from fracture, but also protects the skull from injury. The evolution of the horns from the Bovidae family makes them sophisticated impact resistant structures, to accommodate their fighting behaviors.

In contrast to the ambient dry horn stress-strain curves, Figure 30 shows the compressive strain-stress curves in the rehydrated state. The maximum compressive stress drops severely for all orientations and has a negative relationship to increasing water content. The mechanical properties of the rehydrated horns are shown in Table 7. Given the significant decrease of all mechanical properties over those of the dry horns, hydration is demonstrated to significantly influence the mechanical response. Comparing the four horns, the strength, stiffness, resilience and toughness drop more conspicuously in the pronghorn, which has the highest water content in the rehydrated condition.

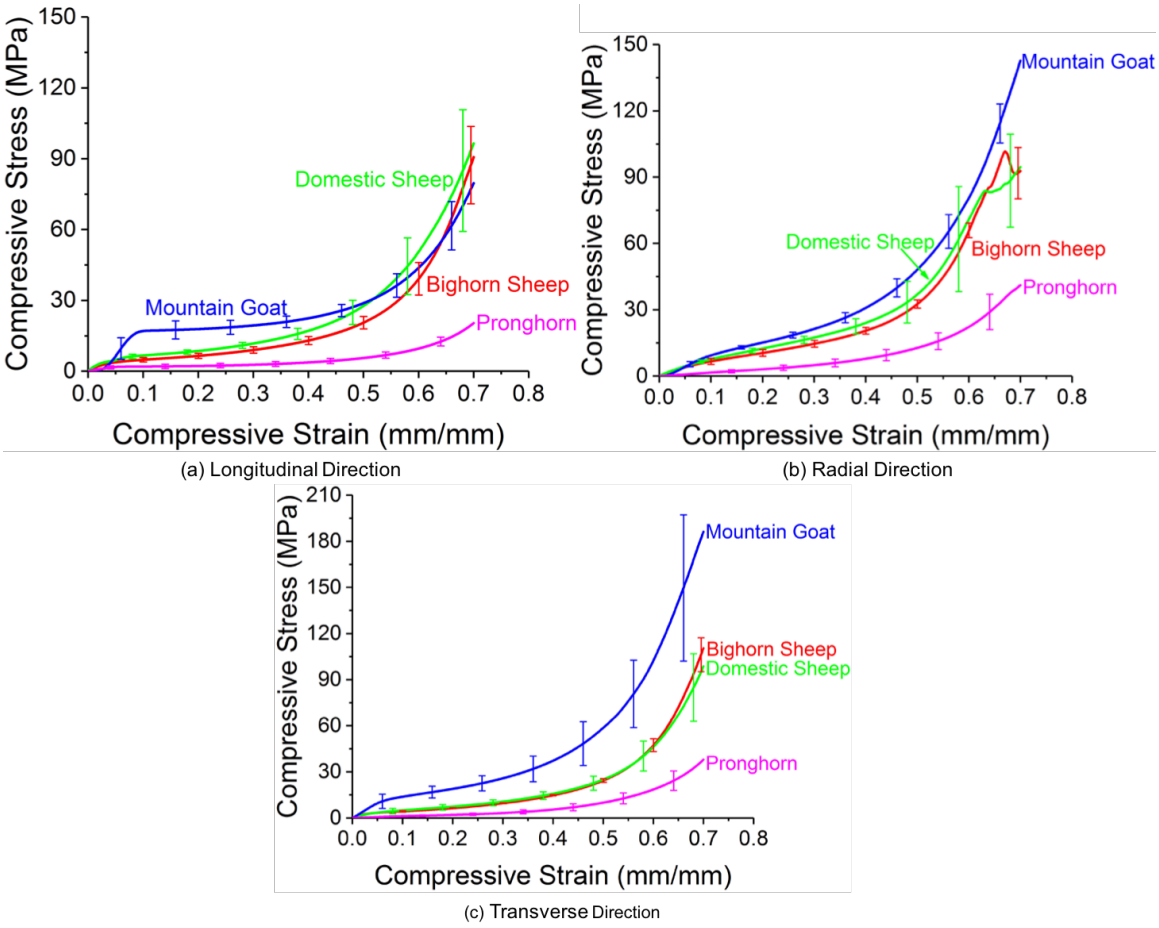

Figure 30. Compressive stress-strain curves comparison of rehydrated horns in the **(a)** longitudinal, **(b)** radial and **(c)** transverse directions. The yield and ultimate strength of the pronghorn horn is much smaller than the other horns. (n = 5)

Table 7. Water content, Young's modulus, yield strength, resilience and toughness of fully rehydrated horns.

Species	Pronghorn	Bighorn sheep	Domestic sheep	Mountain goat
Water content (ambient condition, wt.%)	44	32	29	24
Young's modulus (longitudinal direction, GPa)	0.11±0.04	0.14±0.08	0.26±0.13	0.50±0.23
Young's modulus (radial direction, GPa)	0.02±0.007	0.09±0.04	0.11±0.03	0.14±0.03
Young's modulus (transverse direction, GPa)	0.02±0.003	0.16±0.05	0.15±0.06	0.23±0.14
Yield strength (longitudinal direction, MPa)	1.6±0.9	3.4±0.8	4.9±1.1	13.9±4.1
Yield strength (radial direction, MPa)	1.7±0.5	5.2±0.6	5.4±0.5	8.6±0.8
Yield strength (transverse direction, MPa)	1.0±0.3	3.2±0.4	3.6±1.1	7.2±1.7
Resilience (longitudinal direction, MJ/m^3)	0.03±0.02	0.08±0.03	0.09±0.04	0.3±0.08
Resilience (radial direction, MJ/m^3)	0.08±0.04	0.2±0.03	0.2±0.04	0.3±0.07
Resilience (transverse direction, MJ/m^3)	0.04±0.01	0.07±0.02	0.06±0.02	0.2±0.1
Toughness (longitudinal direction, MJ/m^3)	3.5±0.7	13.3±1.7	16.7±3.6	18.4±2.7
Toughness (radial direction, MJ/m^3)	7.2±1.5	20.1±1.1	21.5±5.3	27.1±2.6
Toughness (transverse direction, MJ/m^3)	6.8±0.4	15.5±1.1	15.4±3.5	26.5±2.0

The amount of the energy absorbed during the compressing process was taken as the area under the strain-stress curves up to 70% strain. As shown in Figure 31, for the dry horns (solid lines), the radial direction can absorb more compressive energy than in the longitudinal and transverse directions. This is because the lamellae are layered face-to-face along radial direction (shown in Figure 10 (d)), which allows them to be withstand more compressive stress without overly deforming. The radial direction is also the orientation in

which the sheep horns clash during the combat. In all directions, the mountain goat horn exhibits the largest energy absorption compared to the other horns. The nearly zero porosity in the mountain goat horn and parallel alignment of the lamella in the longitudinal direction may be the factors influencing the energy absorption ability. Bighorn sheep also possess high energy absorption capability, especially along the radial direction. During combat, the bighorn sheep tend to clash into each other's horns with a high speed. The high energy absorption ability prevents horns from cracking and crushing when subjected to high impact loads. When the horns are fully rehydrated, the energy absorbed decreases dramatically (Figure 31 dashed lines), which is probably due to the seriously softening of the matrix. Also, the difference of energy absorbing ability between different loading directions diminishes, which indicates a matrix dominant property for rehydrated horns.

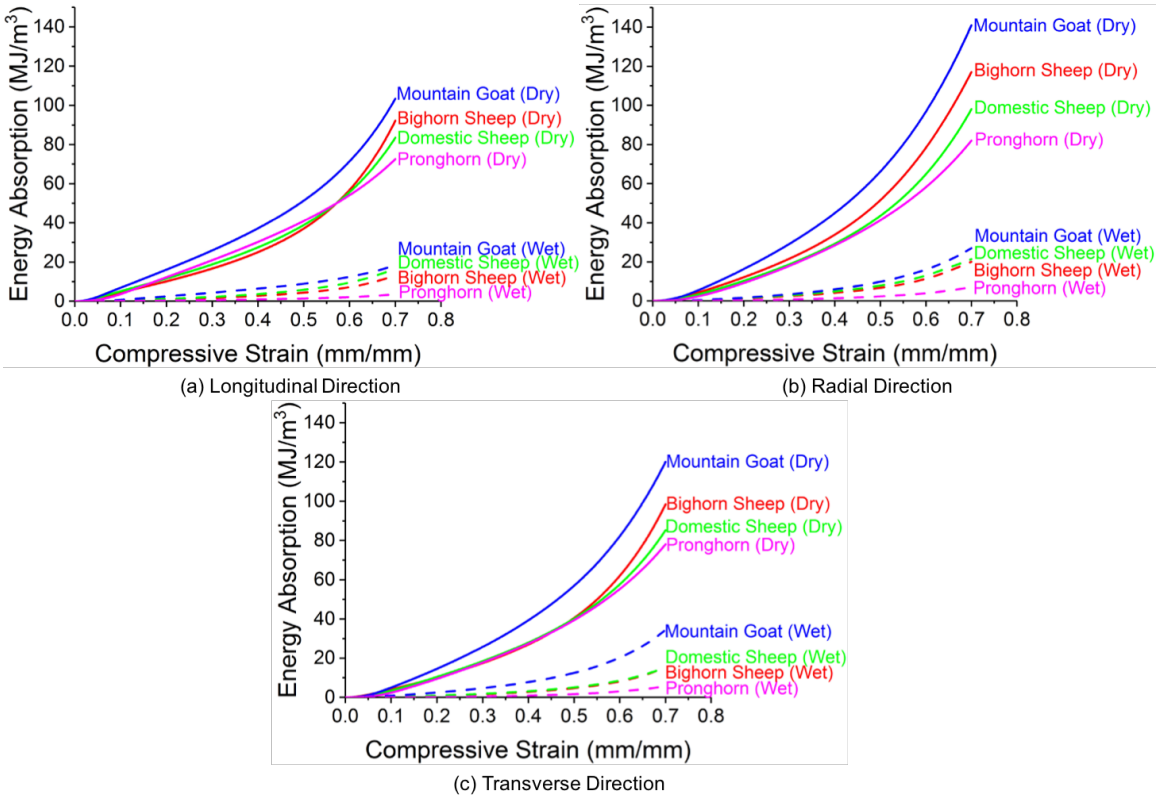

Figure 31. Energy absorption with the compressive strain of dry and rehydrated horns in the **(a)** longitudinal, **(b)** radial and **(c)** transverse directions. (n = 5)

The relationship between hydration level and mechanical properties in three loading directions are shown in Figure 32, with each water content corresponded to a horn from the four species (in an order of mountain goat, domestic sheep, bighorn sheep and pronghorn) in either ambient or fully rehydrated status. For ambient dry horns, when comparing the different loading directions, the longitudinal direction has the highest Young's modulus (Figure 32 (a)) and yield strength (Figure 32 (b)), which indicates the strongest direction of the horn. The radial direction has the largest resilience (Figure 32 (c)) and toughness (Figure 32 (d)), which indicates the most energy absorbing direction of the horn. For all orientations, the mechanical properties decrease dramatically with increasing

water content. With an increased hydration level, the differences of the mechanical properties between directions is significantly reduced, which suggests that hydration severely degraded the matrix phase that dominates the deformation behavior. This is in accordance with the plasticizing effect of increasing water content in the matrix [73]. It can be concluded that the change between hard (dry) and ductile (hydrated) horns can be manipulated by changing the water content of the structure. All species present hydration dominated mechanical properties of their horns, which indicates a common characteristic for the horns.

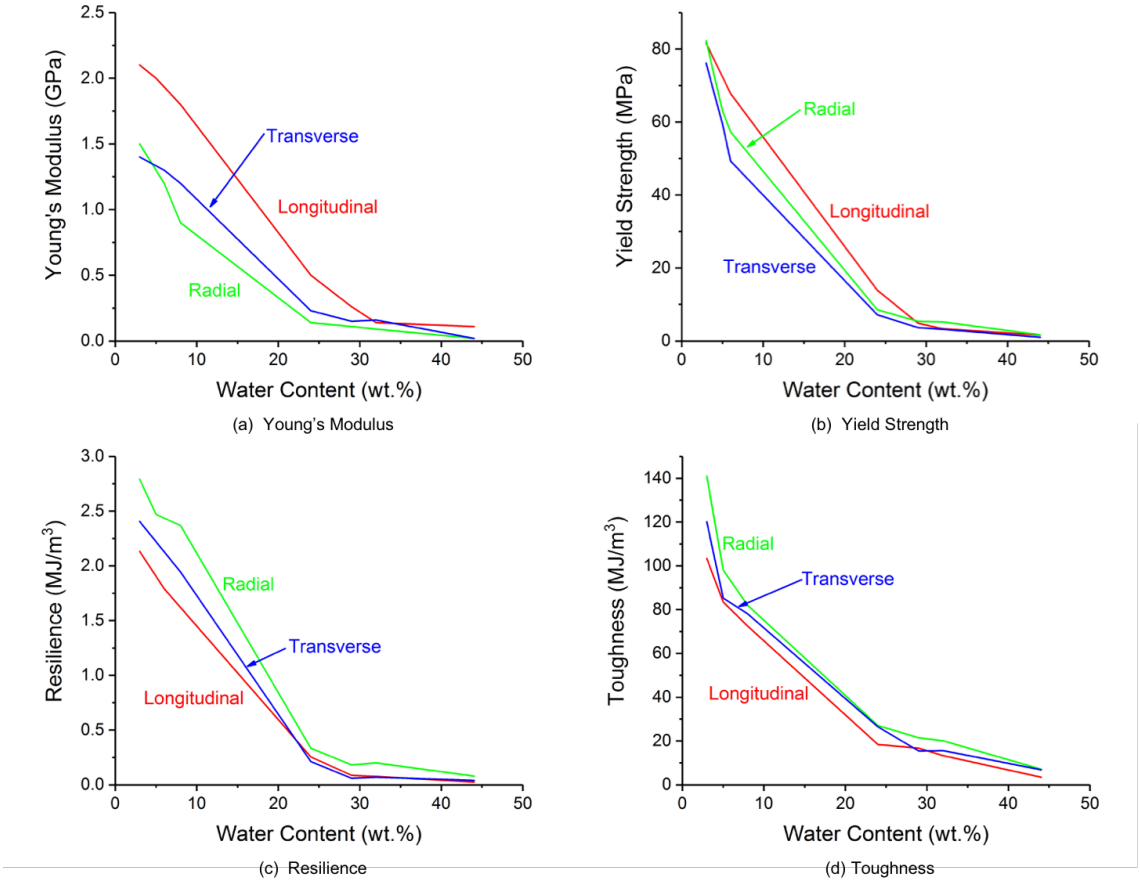

Figure 32. (a) Young's modulus, **(b)** yield strength, **(c)** resilience and **(d)** toughness as a function of water content of horns from mountain goat, domestic sheep, bighorn sheep and pronghorn (each water content corresponded to a certain kind of horn from four species) in the longitudinal, radial and transverse directions.

5.2.2 Tensile Tests

Tensile test was performed only along longitudinal direction because it is the most likely direction to undergo tensile stress when impact occurs. Only ambient dried horns were tested. The stress-strain curves are shown in Figure 33. As shown in the figure, the mountain goat has the largest failure strain (14.7%), while the domestic sheep has the smallest (5.9%). The failure strain in tension is much smaller than in compression, which indicates a different fracture mechanism. The mechanical properties of the horns under the tensile stress are listed in Table 8. Among the four horns, the mountain goat is the stiffest (1.54 GPa), strongest (yield strength of 88.0 MPa and ultimate strength 107.3 MPa), toughest (11.9 MJ/m^3) and most resilient (2.75 MJ/m^3). This may be linked to mountain goat stabbing combat style. The horns may be subjected to tensile stresses when the goat tries to pull its horns out from others body [76]. When pulling the horns out, a friction force is generated between soft tissue and horn. A high yield strength maintains structural integrity while stabbing and avoids large plastic deformation. The pronghorn has the second strongest (yield strength of 69.6 MPa and ultimate strength of 78.3 MPa) and toughest (6.1 MJ/m^3) horn. Since the pronghorn performs two methods of combat, one involving thrusting and twisting where tensile stress will be generated. To avoid neck injury, this would be an important property. For bighorn and domestic sheep, since they do not involve in stabbing behavior, the yield strengths are lower (38.9 GPa for bighorn and 41.9 GPa for domestic sheep) compared to the mountain goat and pronghorn. The bighorn sheep horn also has a small fracture strain of 6.5%, while domestic sheep horn shows similar property – a fracture strain of 5.9%.

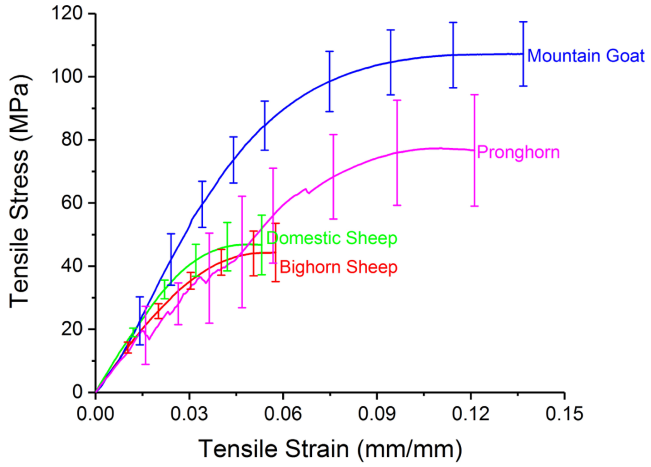

Figure 33. Average (n = 7) longitudinal tensile stress-strain response for the horns. Specimen are in the ambient dry condition.

Table 8. Longitudinal tensile mechanical properties of ambient dry horns.

Species	Pronghorn	Bighorn sheep	Domestic sheep	Mountain goat
Young's modulus (GPa)	1.06±0.2	1.15±0.1	1.33±0.1	1.54±0.2
Yield strength (MPa)	69.6±12.3	38.9±7.3	41.9±9.9	88.0±12.5
Resilience (MJ/m^3)	2.40±1.2	0.78±0.2	0.75±0.2	2.75±0.5
Ultimate Strength (MPa)	78.3±14.9	45.1±10.5	47.9±11.5	107.3±9.8
Failure Strain (%)	11.9±1.5	6.5±1.2	5.9±1.4	14.7±1.8
Toughness (MJ/m^3)	6.1±1.6	2.3±0.7	2.1±0.9	11.9±1.7

Since the lamellae of mountain goat and pronghorn have the lamella faces parallel to the tubule growth direction (Figure 21 (c) and (d)), while bighorn sheep horn and domestic sheep horn have the lamellae arranged at angles to tubules (Figure 21 (a) and (b)), it appears that the mechanical properties increase as the lamellae align more parallel to tubule direction. In addition, the keratin cell shape may also influence the yield strength. The keratin cells of mountain goat and pronghorn horns are thinner and more regularly

shaped, while cells from bighorn sheep and domestic sheep have sharp arcs and protuberances.

Compared to compressive tests at same hydration level (ambient dry) and load direction (longitudinal), the tensile failure strain and stress decrease significantly. Under compressive stress, the horn can have a deformation of 70% without failure. However, under tensile stress, the horn fractures when the strain is > 15%. The horns can be subjected to a compressive stress of 500 MPa without failure while the ultimate tensile strength of the horn is four times lower. The energy absorption ability also decreases due to the decreasing of failure strain and stress, indicating a more brittle characteristic when the horn is under tensile load.

SEM images of fracture surfaces under tension are shown in Figure 34. For all horns, tubule pull-out is rarely observed, which indicates a high tubule-to-matrix adhesion. However, fiber-to-fiber adhesion may be one factor that influences the tensile properties. For horns having a relatively low yield strength (bighorn sheep) (Figure 34 (a) and (b)) and domestic sheep (Figure 34 (c) and (d))), detachment of the fiber bundles from the matrix is observed. The detached fibers are thin with a small diameter of 1-1.5 μm. High stresses applied on those thin fibers causes fiber fracture at a relatively low tensile load. For horns having a high yield strength (mountain goat (Figure 34 (e) and (f))), detached fibers are not observed, thus a good fiber-matrix adhesion is expected. For the pronghorn, which also has a high yield strength, there is separation between the fiber bundles and the matrix, but the detached fiber bundles have a larger diameter (> 10 μm). Compared to thin fibers observed the bighorn sheep and domestic sheep, these thick fibers are stronger under the same load and can withstand more tensile stress.

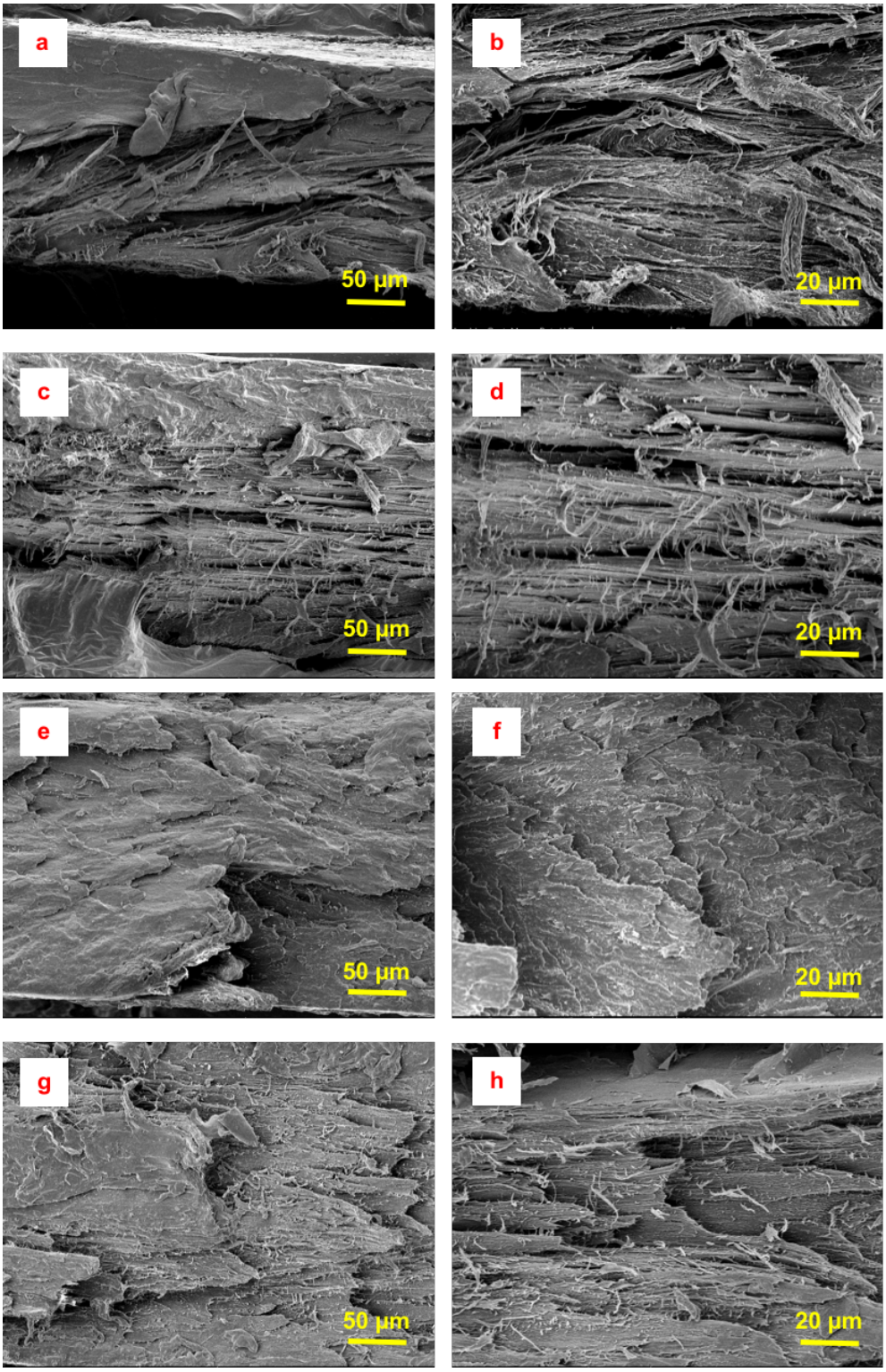

Figure 34. Scanning electron microscopy images of tensile fracture surfaces of the horns. The left are low magnification images and the right are high magnification images. **(a,b)** bighorn sheep, **(c,d)** domestic sheep **(e,f)** mountain goat and **(g,h)** pronghorn.

5.2.3 Impact Tests

Since the size and keratin sheath thickness limitation of pronghorn and mountain goat, only bighorn sheep and domestic sheep samples were prepared and tested. According to ASTM standard D7136/D7136 M-07 [78], there are four externally visible damage types and two internal damage types appearing in drop-weight test, shown in Figure 35. Dent (depression), splits (cracks), combined splits and delamination, and puncture are four externally visible damage types. Internal damage types are sorted into two categories: delamination and splits (cracks). Dimpling is the main damage mode on the impact surface for both sheep horns. With an increase in the impact energy, the diameter and depth of dimple increases. On the bottom surface, from low to high impact energy, the domestic sheep horn shows all external damage types. For bighorn sheep, on the bottom surface only split/crack, delamination and puncture were observed.

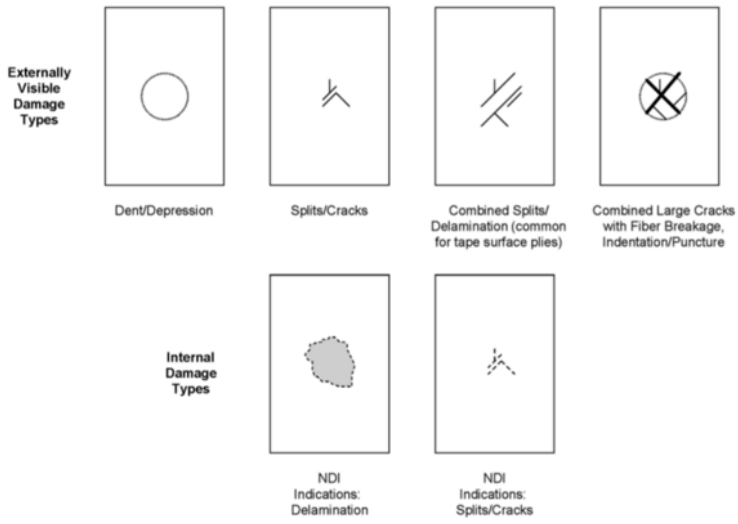

Figure 35. Commonly observed damage modes after a drop tower test. External damage modes: dent/depression, splits/cracks, combined splits/delamination, combined large cracks with fiber breakage, indentation/puncture, which are applied to both impact surface and bottom surface. Internal damage modes: delamination, splits/cracks. NDI represents for non-destructive inspection method. Taken from [78].

The typical damage modes under low and high normalized impact energy (E_n) of bighorn and domestic sheep is shown in Figure 36. At low E_n (30 kJ/m^2), shown in Figure 36 (a) and (c), for both horns there is a shallow dimple on top (impact) surface with an area same as the size of the hemispherical impactor tip (3.2 mm). On the bottom, the domestic sheep has a minor crack (crack length of 3 mm), while the bighorn sheep horn exhibits a longer crack (crack length of 10 mm), which indicates that domestic sheep can sustain more stress and exhibit a lighter damage when E_n is small. At high E_n (60 kJ/m^2), for both horns a number of samples failure and the typical failure modes are exhibited in Figure 36 (b) and (d). On the bottom, for the domestic sheep, circular and thin chips fractured away from the surface, while for the bighorn sheep thin chips were only punched out but not fractured away. Also, there is a delamination combined with the dimple revealed on the top of domestic sheep, which means that at high E_n level, bighorn sheep reveals a higher capability to suffer the impact load. The number of each damage mode under the same E_n is shown in Figure 37. The bighorn sheep begins to fail when E_n = 40 kJ/m^2, whereas there is no failure damage for domestic sheep at this energy level, which also indicates a higher impact resistance of domestic sheep under low impact speed. According to definition of failure impact strength given by Lee, et. al [22], failure impact strength is defined when 50% of the samples fail (with failure defined when the bottom surface of the sample shows puncture damage). The failure impact strength of domestic sheep is 55 kJ/m^2. The bighorn sheep has a higher failure impact strength of 75 kJ/m^2, 36% more than domestic sheep. The failure impact strength reveals that the bighorn sheep has better impact resistance when the impact speed is high. Domestic and bighorn sheep have similar fighting styles, but with different fighting speeds. When fighting, domestic sheep stand closer to each other than

bighorn sheep, thus generating a lower speed for clashing. The impact test results suggest that the evolution of horn properties are to fit fighting behavior.

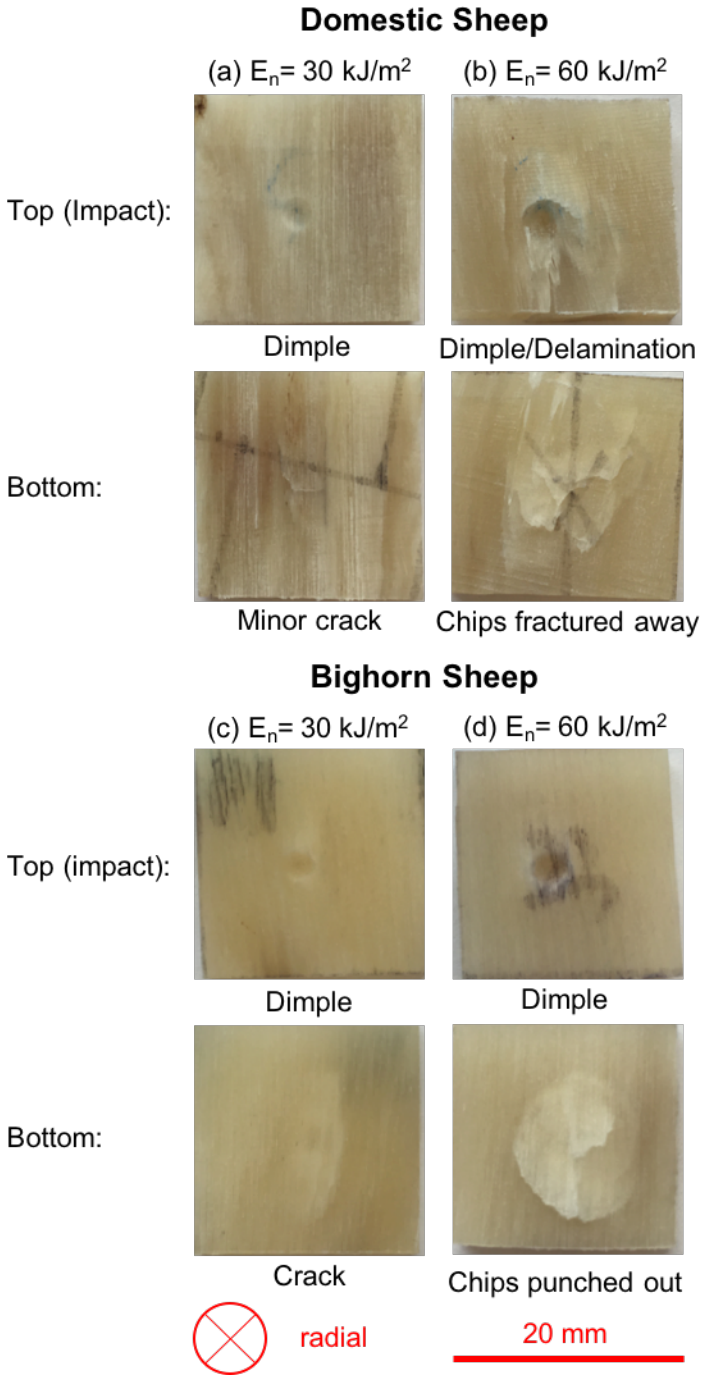

Figure 36. External damage modes of **(a)** and **(b)** domestic sheep and **(c)** and **(d)** bighorn sheep with associated normalized impact energy (E_n). Radial direction points out of the page. Black lines are from a pen.

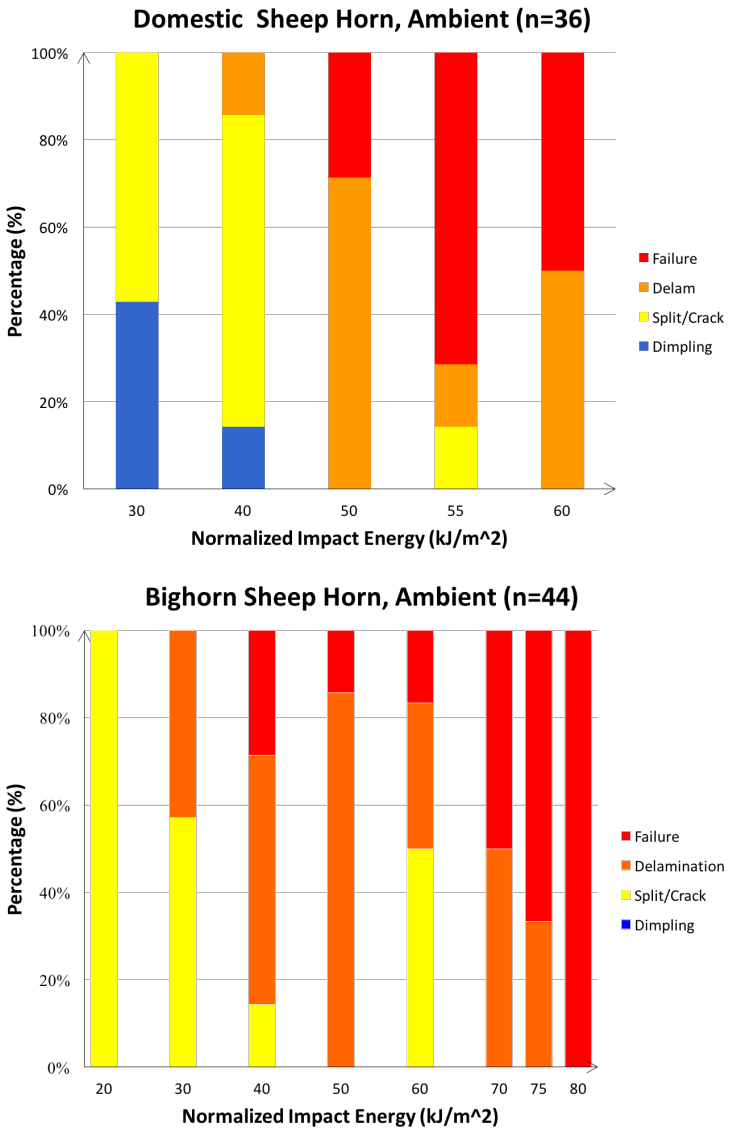

Figure 37. Damage types (bottom surface) with different normalized impact energy from the **(a)** domestic sheep and **(b)** bighorn sheep horn.

6 Conclusions

The Bovidae family (sheep and goat) and Antilocapridae family (pronghorn) do not share the same origin, but the two families have similarities in their behavior and horn microstructures [26]. The microstructure and mechanical properties of bighorn sheep horn have been studied in the past. However, the investigation of horns from other artiodactyl members is lacking. Domestic sheep and bighorn sheep are close relatives from same genus [79]. The mountain goat is from the same family but a different subfamily. The pronghorn is the only existing species in Antilocapridae family and share similar characteristics with the Bovidae family [26]. This thesis compared the microstructures and mechanical properties of keratin horns from four different species—bighorn sheep, domestic sheep, pronghorn and mountain goat. Microstructural analysis was accomplished by optical and scanning electron microscopy. Mechanical properties comparison was performed by quasi-static compression tests (dry and rehydrated conditions), quasi-static tension tests and drop tower impact tests.

Optical microscopy characterized the keratin cell alignment and tubule distribution. Elliptically-shaped tubules (major axis ~ 70-80 μm, minor axis ~ 10-20 μm) that extend in the growth direction are present in the sheep and pronghorn; whereas tubules were not identified in the mountain goat. The bighorn sheep horn has the highest porosity (from the presence of the tubules) of 11.3%. The porosity of domestic sheep horn is 7.7% and the tubules have a deformed oval shape. The pronghorn horn has a porosity of 5.8% and the porosity of mountain goat horn is nearly 0. In all horns, keratin cells (disk-shaped) align along longitudinal direction with their edges, forming a lamella, and the lamellae layered

along radial direction with their faces forming a wavy pattern surrounding the tubules. The pronghorn and mountain goat horn lamellae align parallel to longitudinal direction and show a high tensile strength. The bighorn sheep horn lamellae arrange 41° to tubule extending direction and the domestic sheep horn has a more disordered alignment, resulting in lower tensile strengths for the sheep compared to the pronghorn and mountain goat. The cell shape is also slightly different and may have an influence on the mechanical properties. Some cells in the bighorn and domestic sheep have an irregular shape with sharp arcs, while cells in the mountain goat and pronghorn have a larger length to width ratio. Further experiments are needed to verify this hypothesis.

The pronghorn horn has the largest water containing ability with a maximum of 44%, that may be caused by the additional water stored in the nanopores inside the keratin cell. The maximum water content of the bighorn sheep, domestic sheep and mountain goat are similar at 32%, 29% and 24%, respectively. This high water absorption ability shows that horns, even without the presence of tubules, absorb water in the keratin matrix.

Compression tests (to 70% strain) reveal similar mechanical properties in the horns. All the horns have anisotropic behavior related to loading direction: longitudinal (direction of tubules), radial (direction of impact) and transverse (perpendicular to both). In the dry condition, the longitudinal direction has the highest Young's modulus and yield strength, since the tubules and lamella align parallel to loading direction. The radial direction has the largest resilience and toughness, facilitated by lamellae layered parallel to the radial direction. No obvious difference is found for the Young's modulus and resilience of different horns, which indicates they are matrix-dominant properties. The water content of the horns has a significant influence on the mechanical properties. With increasing water

content, all mechanical properties decreased. The pronghorn has a significantly lower ultimate strength compared to the other horns in the rehydrated condition. This may be attributed to (a) nanopores in the keratin cells, (b) the large aspect ratio of the cells and (c) the pronghorn is from a different family from the others. The results prove that the anisotropic behavior and hydration-dominated mechanical properties are common characteristics of keratin horns. Scanning electron microscopy analyses deformation and failure mechanisms. Buckling and delamination are main deformation modes under compressive stress. Cracks propagate along maximum shear stress direction. Cracks in the bighorn sheep, pronghorn and domestic sheep horns are long and wide, while in mountain goat cracks are short and narrow.

Under compressive stress, the mountain goat horn has highest stiffness and energy absorption in all directions, both in ambient condition and rehydrated conditions. Tension tests also reveal these horns have the highest tensile strength. This stiff and tough horn is optimal for its stabbing combat style. Bighorn sheep also possess high energy absorption capability under compressive load, especially along radial direction, which makes them suitable for absorbing energy generated by clashing, giving protection to the skull. The relatively low tensile strength of bighorn and domestic sheep indicates that their horns are mostly subjected to compressive rather than tensile stress. The pronghorn horn shows relatively high energy absorption in compression tests and large tensile strength. This mechanical response is optimal for clashing combat and interlocking horn fighting behavior. Scanning electron microscopy images of fracture surfaces under tension reveals that fiber-fiber adhesion is one factor influencing the tensile mechanical properties of the horns.

Drop weight impact tests compared the impact resistance of the bighorn and domestic sheep horns. At low normalized impact energy (< 40 kJ/m^2), dimpling exists as a damage mode on the bottom surface of the domestic sheep samples, but no dimpling occured on the bottom surface of the bighorn sheep samples. With increasing normalized impact energy, the domestic sheep horn exhibits delamination damage mode combined with large cracks, while bighorn sheep horn exhibits only delamination and small cracks. Under low normalized impact energy, the domestic sheep has higher impact resistance than the bighorn sheep. At high normalized impact energy (> 55 kJ/m^2), the bighorn sheep has better impact resistance. The failure impact strength of domestic sheep is 55 kJ/m^2 and the impact strength of bighorn sheep is 75 kJ/m^2. The result indicates that bighorn sheep have developed horns to survive large impact forces.

Revisiting the hypotheses of the thesis, it has been found that similarities exist in different horn microstructures while cell alignment and tubule distribution differ from each other, and the variations can explain their mechanical properties differences. Keratin horn is a hydration-dominated material. Relationships between structure, mechanical properties and fighting behavior were elucidated.

7 Recommendations for Future Research

Since this is the first time comparing four keratin horns from different species, there is much more to understand about the similarity and differences of horns from different species. How the microstructure and mechanical properties of horns accommodate to their fighting behavior is also an interesting area to investigate. Work that can be performed in the future include:

- Determine the orientation of intermediate filaments inside keratin cell, which could be observed under transmission electron microscopy. This may help explain differences in mechanical properties.
- Study the microstructure of mountain goat horn under nano-computed tomography that could possibly verify the existence of tubules, which are not observed in the present study.
- Confirm the keratin cell shape using nano-computed tomography to obtain 3D images.
- Perform compression tests *in-situ* in the scanning electron microscope to fully understand the crack propagation and delamination mechanisms.
- Equip present drop machine with force and displacement detector, to obtain strain-stress curves of impact tests.

Appendix

Appendix I. Optical Microscopy Sample Preparation Protocol

1. Use a section saw to cut horns into 2 mm x 2 mm x 4 mm cuboids. Choose one cross section with a 2 mm x 2 mm area as the designated surface and 4 mm is the thickness of the sample.
2. Use the side surface of the saw to polish the designated surface. This is to smooth the surface so that it will be easier to cut in the Ultramicrotome.
3. Mix epoxy and hardener by a volume proportion of 4:1 in a plastic container. Leave overnight to let the epoxy harden.
4. Tear the plastic container off and use section saw to cut epoxy into 4 mm x 4 mm x 10 mm cuboids.
5. Use 409 Liquid Glue to tight the opposite surface of designated surface onto the cross section of epoxy cuboids. Stand in air for 5 min to dry the glue.
6. Fix the epoxy into sample holder of Ultramicrotome, with the designated surface on the top and parallel to the surface of sample holder. Install sample holder on cutting machine. Then install triangle-shape glass blade on blade holder. Place blade holder on cutting machine.
7. Use manual control mode to cut thin slices off the horn surface until no scratches are seen on the surface.
8. Prepare a glass slide. Add 4 to 5 purified water drops to slide. Change into rolling feeding mode. Set feeding distance per rolling to 1200 nm. Slowly and smoothly roll the handle one circle to cut one slice off. Use pointed tweezer gently

transferring slice onto one water drop. Repeat the cutting and transferring procedure several times until all water drops have a slice on it.

9. Preheat hot template to 200˚C. Put glass slide on hot template until water fully evaporate. Take the slide off and add Toluidine blue stain ((a basic thiazine metachromatic dye with high affinity for acidic tissue components)) drops on each thin slice and stand in room temperature for 2 to 3 min, depending on different horns. Gently wash the stain off using purified water. Put the glass slide back on hot template until the slide is fully dried.
10. Take the slide off and let it cool down to room temperature.
11. Observe the slide under optical microscope.

References

[1] M. Ashby, L. Gibson, U. Wegst, R. Olive, The mechanical properties of rnatural materials. I. Material property charts, Proceedings of the Royal Society of London A: Mathematical, Physical and Engineering Sciences, The Royal Society, 1995, pp. 123-140.

[2] U. Wegst, M. Ashby, The mechanical efficiency of natural materials, Philosophical Magazine 84(21) (2004) 2167-2186.

[3] L. Szewciw, D. De Kerckhove, G. Grime, D.S. Fudge, Calcification provides mechanical reinforcement to whale baleen α-keratin, Proceedings of the Royal Society of London B: Biological Sciences 277(1694) (2010) 2597-2605.

[4] M.A. Meyers, P.-Y. Chen, A.Y.-M. Lin, Y. Seki, Biological materials: structure and mechanical properties, Progress in Materials Science 53(1) (2008) 1-206.

[5] L. Pauling, R.B. Corey, Compound helical configurations of polypeptide chains: structure of proteins of the α-keratin type, Nature 171(4341) (1953) 59-61.

[6] T.-T. Sun, R. Eichner, W.G. Nelson, C.S. Tseng, R.A. Weiss, M. Jarvinen, J. Woodcock-Mitchell, Keratin classes: molecular markers for different types of epithelial differentiation, Journal of Investigative Dermatology 81(1) (1983) S109-S115.

[7] M. Feughelman, Mechanical Properties and Structure of Alpha-keratin Fibres: Wool, Human Hair and Related Fibres, UNSW Press, Sydney, Australia, 1997.

[8] B. Filshie, G. Rogers, An electron microscope study of the fine structure of feather keratin, The Journal of Cell Biology 13(1) (1962) 1-12.

[9] R. Fraser, T. MacRae, G.E. Rogers, Keratins: their composition, structure, and biosynthesis, Charles C. Thomas1972.

[10] G. Rogers, Electron microscopy of wool, Journal of ultrastructure research 2(3) (1959) 309-330.

[11] G. Rogers, Electron microscope studies of hair and wool, Annals of the New York Academy of Sciences 83(1) (1959) 378-399.

[12] J. Woods, D. Harland, J. Vernon, G. Krsinic, R. Walls, Morphology and ultrastructure of antler velvet hair and body hair from red deer (Cervus elaphus), Journal of morphology 272(1) (2011) 34-49.

[13] I. Brody, The ultrastructure of the tonofibrils in the keratinization process of normal human epidermis, Journal of Ultrastructure Research 4(3-4) (1960) 264-297.

[14] M.A. Kasapi, J.M. Gosline, Design complexity and fracture control in the equine hoof wall, Journal of Experimental Biology 200(11) (1997) 1639-1659.

[15] M.-C.G. Klein, J.K. Deuschle, S.N. Gorb, Material properties of the skin of the Kenyan sand boa Gongylophis colubrinus (Squamata, Boidae), Journal of Comparative Physiology A 196(9) (2010) 659-668.

[16] T. Lingham-Soliar, N. Murugan, A new helical crossed-fibre structure of β-keratin in flight feathers and its biomechanical implications, PloS one 8(6) (2013) e65849.

[17] L. Tombolato, E.E. Novitskaya, P.-Y. Chen, F.A. Sheppard, J. McKittrick, Microstructure, elastic properties and deformation mechanisms of horn keratin, Acta Biomaterialia 6(2) (2010) 319-330.

[18] L. Farren, S. Shayler, A. Ennos, The fracture properties and mechanical design of human fingernails, Journal of Experimental Biology 207(5) (2004) 735-741.

[19] Y. Seki, M.S. Schneider, M.A. Meyers, Structure and mechanical behavior of a toucan beak, Acta Materialia 53(20) (2005) 5281-5296.

[20] K. Johnson, M. Trim, D. Francis, W. Whittington, J. Miller, C. Bennett, M. Horstemeyer, Moisture, anisotropy, stress state, and strain rate effects on bighorn sheep horn keratin mechanical properties, Acta Biomaterialia 48 (2017) 300-308.

[21] K.E. Ruckstuhl, Foraging behaviour and sexual segregation in bighorn sheep, Animal Behaviour 56(1) (1998) 99-106.

[22] S. Lee, E.E. Novitskaya, B. Reynante, J. Vasquez, R. Urbaniak, T. Takahashi, E. Woolley, L. Tombolato, P.-Y. Chen, J. McKittrick, Impact testing of structural biological materials, Materials Science and Engineering: C 31(4) (2011) 730-739.

[23] M.W. Trim, M. Horstemeyer, H. Rhee, H. El Kadiri, L.N. Williams, J. Liao, K.B. Walters, J. McKittrick, S.-J. Park, The effects of water and microstructure on the mechanical properties of bighorn sheep (Ovis canadensis) horn keratin, Acta Biomaterialia 7(3) (2011) 1228-1240.

[24] S. Hiendleder, B. Kaupe, R. Wassmuth, A. Janke, Molecular analysis of wild and domestic sheep questions current nomenclature and provides evidence for domestication from two different subspecies, Proceedings of the Royal Society of London B: Biological Sciences 269(1494) (2002) 893-904.

[25] K.L. Risenhoover, J.A. Bailey, Relationships between group size, feeding time, and agonistic behavior of mountain goats, Canadian Journal of Zoology 63(11) (1985) 2501-2506.

[26] D.W. Kitchen, Social behavior and ecology of the pronghorn, Wildlife Monographs (38) (1974) 3-96.

[27] P.A. Coulombe, M.B. Omary, 'Hard'and 'soft'principles defining the structure, function and regulation of keratin intermediate filaments, Current Ppinion in Cell Biology 14(1) (2002) 110-122.

[28] H. Herrmann, U. Aebi, Intermediate filaments: molecular structure, assembly mechanism, and integration into functionally distinct intracellular scaffolds, Annual Review of Biochemistry 73(1) (2004) 749-789.

[29] W.T. Astbury, W.A. Sisson, "X-ray studies of the structure of hair, wool, and related fibres. III. The configuration of the keratin molecule and its orientation in the biological cell." Proceedings of the Royal Society of London. Series A, Mathematical and Physical Sciences 150.871 (1935): 533-551.

[30] R. Fraser, T. MacRae, The structure of α-keratin, Polymer 14(2) (1973) 61-67.

[31] R. Fraser, T. MacRae, D. Parry, E. Suzuki, The structure of β-keratin, Polymer 10 (1969) 810-826.

[32] R.B. Fraser, D.A. Parry, The structural basis of the filament-matrix texture in the avian/reptilian group of hard β-keratins, Journal of Structural Biology 173(2) (2011) 391-405.

[33] L. Harvey, D. Baltimore, A. Berk, S.L. Zipursky, P. Matsudaira, J. Darnell, Molecular Cell Biology. Vol. 3. New York: Scientific American Books, 1995.

[34] R. Fraser, T.P. MacRae, D. Parry, E. Suzuki, Intermediate filaments in alpha-keratins, Proceedings of the National Academy of Sciences 83(5) (1986) 1179-1183.

[35] P.M. Steinert, R.H. Rice, D.R. Roop, B.L. Trus, A.C. Steven, Complete amino acid sequence of a mouse epidermal keratin subunit and implications for the structure of intermediate filaments, Nature 302 (1983) 794-800.

[36] J. Squire, P.J. Vibert, Fibrous Protein Structure, Academic Press, 1987.

[37] J. McKittrick, P.-Y. Chen, S. Bodde, W. Yang, E. Novitskaya, M. Meyers, The structure, functions, and mechanical properties of keratin, JOM 64(4) (2012) 449-468.

[38] N.E. Waters, The Mechanical Properties of Biological Materials: Symposia of the Society for Experimental Biology (edited by J.F.V. Vincent and J.D. Currey), Vol. 24, Cambridge University Press, Cambridge, United Kingdom, 1980.

[39] B. Chapman, A review of the mechanical properties of keratin fibres, Journal of the Textile Institute 60(5) (1969) 181-207.

[40] J. McKittrick, P.-Y. Chen, L. Tombolato, E. Novitskaya, M. Trim, G. Hirata, E. Olevsky, M. Horstemeyer, M. Meyers, Energy absorbent natural materials and bioinspired design strategies: a review, Materials Science and Engineering: C 30(3) (2010) 331-342.

[41] L. Jones, M. Simon, N. Watts, F. Booy, A. Steven, D. Parry, Intermediate filament structure: hard α-keratin, Biophysical Chemistry 68(1-3) (1997) 83-93.

[42] P.M. Steinert, D.A. Parry, Intermediate filaments: conformity and diversity of expression and structure, Annual Review of Cell Biology 1(1) (1985) 41-65.

[43] R.S. Bear, H.J. Rugo, The results of x-ray diffraction studies on keratin fibers, Annals of the New York Academy of Sciences 53(1) (1951) 627-648.

[44] B. Busson, F. Briki, J. Doucet, Side-chains configurations in coiled coils revealed by the 5.15-Å meridional reflection on hard α-keratin X-ray diffraction patterns, Journal of Structural Biology 125(1) (1999) 1-10.

[45] P.-Y. Chen, J. McKittrick, M.A. Meyers, Biological materials: functional adaptations and bioinspired designs, Progress in Materials Science 57(8) (2012) 1492-1704.

[46] B. Wang, W. Yang, J. McKittrick, M.A. Meyers, Keratin: Structure, mechanical properties, occurrence in biological organisms, and efforts at bioinspiration, Progress in Materials Science 76 (2016) 229-318.

[47] M. Feughelman, M. Robinson, The relationship between some mechanical properties of single wool fibers and relative humidity, Textile Research Journal 37(6) (1967) 441-446.

[48] D.S. Fudge, K.H. Gardner, V.T. Forsyth, C. Riekel, J.M. Gosline, The mechanical properties of hydrated intermediate filaments: insights from hagfish slime threads, Biophysical Journal 85(3) (2003) 2015-2027.

[49] J. Bertram, J. Gosline, Functional design of horse hoof keratin: the modulation of mechanical properties through hydration effects, Journal of Experimental Biology 130(1) (1987) 121-136.

[50] D.S. Fudge, J.M. Gosline, Molecular design of the α–keratin composite: insights from a matrix–free model, hagfish slime threads, Proceedings of the Royal Society of London B: Biological Sciences 271(1536) (2004) 291-299.

[51] A. Kitchener, Fracture toughness of horns and a reinterpretation of the horning behaviour of bovids, Journal of Zoology 213(4) (1987) 621-639.

[52] R. Fraser, D. Parry, The molecular structure of reptilian keratin, International Journal of Biological Macromolecules 19(3) (1996) 207-211.

[53] E. Bendit, The α–β Transformation in Keratin, Nature 179(4558) (1957) 535-535.

[54] F. Pautard, Mineralization of keratin and its comparison with the enamel matrix, Nature 199(4893) (1963) 531-535.

[55] J. Hearle, A critical review of the structural mechanics of wool and hair fibres, International Journal of Biological Macromolecules 27(2) (2000) 123-138.

[56] B. Chapman, A mechanical model for wool and other keratin fibers, Textile Research Journal 39(12) (1969) 1102-1109.

[57] R. Fraser, T. MacRae, Molecular structure and mechanical properties of keratins, Symposia of the Society for Experimental Biology, 1979, pp. 211-246.

[58] C.-C. Chou, M.J. Buehler, Structure and mechanical properties of human trichocyte keratin intermediate filament protein, Biomacromolecules 13(11) (2012) 3522-3532.

[59] M.A. Kasapi, J.M. Gosline, Strain-rate-dependent mechanical properties of the equine hoof wall, Journal of Experimental Biology 199(5) (1996) 1133-1146.

[60] E. Kjartansson, Constant Q-wave propagation and attenuation, Journal of Geophysical Research: Solid Earth 84(B9) (1979) 4737-4748.

[61] J.D. Currey, Bones: Structure and Mechanics, Princeton University Press, Princeton, New Jersey, USA, 2002.

[62] P.-Y. Chen, A. Stokes, J. McKittrick, Comparison of the structure and mechanical properties of bovine femur bone and antler of the North American elk (Cervus elaphus canadensis), Acta Biomaterialia 5(2) (2009) 693-706.

[63] N. Waters, The mechanical properties of biological materials, Symposia of the Society for Experimental Biology, Cambridge University Press Cambridge, 1980.

[64] L.H. He, N. Fujisawa, M.V. Swain, Elastic modulus and stress–strain response of human enamel by nano-indentation, Biomaterials 27(24) (2006) 4388-4398.

[65] D.H. Leach, The structure and function of the equine hoof wall, Doctoral Dissertation, University of Saskatchewan, Saskatoon, Canada, 1980.

[66] V. Geist, The evolution of horn-like organs, Behaviour 27(1) (1966) 175-214.

[67] A. Kitchener, Fighting and the mechanical design of horns and antlers, Biomechanics in animal behaviour (eds Domenici P., Blake RW). Oxford, UK: BIOS Scientific Publishers Limited (2000).

[68] J.D. Currey, Mechanical properties of bone tissues with greatly differing functions, Journal of Biomechanics 12(4) (1979) 313-319.

[69] J.E. Gordon, Structures, or, Why Things Don't Fall Down, Da Capo Press, Boston, Massachusetts, USA, 2003.

[70] B. Li, H. Zhao, X. Feng, W. Guo, S. Shan, Experimental study on the mechanical properties of the horn sheaths from cattle, Journal of Experimental Biology 213(3) (2010) 479-486.

[71] F. Warburton, Determination of the elastic properties of horn keratin, Journal of the Textile Institute Proceedings 39(7) (1948) P297-P308.

[72] A. Kitchener, J.F. Vincent, Composite theory and the effect of water on the stiffness of horn keratin, Journal of Materials Science 22(4) (1987) 1385-1389.

[73] A. Kitchener, Effect of water on the linear viscoelasticity of horn sheath keratin, Journal of Materials Science Letters 6(3) (1987) 321-322.

[74] V. Geist, Mountain Sheep - A Study in Behavior and Evolution, University of Chicago Press, Chicago, Illinois, USA, 1971.

[75] W.M. Schaffer, Intraspecific combat and the evolution of the Caprini, Evolution (1968) 817-825.

[76] V. Geist, On fighting injuries and dermal shields of mountain goats, The Journal of Wildlife Management (1967) 192-194.

[77] D.W. Kitchen, P.T. Bromley, Agonistic behavior of territorial pronghorn bucks, The behaviour of ungulates and its relation to management. IUCN, Morges, Switzerland (1974) 365-381.

[78] ASTM D7136 / D7136M-07, Standard Test Method for Measuring the Damage Resistance of a Fiber-Reinforced Polymer Matrix Composite to a Drop-Weight Impact Event, ASTM International, West Conshohocken, PA, 2007.

[79] S.H. Forbes, J.T. Hogg, F.C. Buchanan, A.M. Crawford, F.W. Allendorf, Microsatellite evolution in congeneric mammals: domestic and bighorn sheep, Molecular Biology and Evolution 12(6) (1995) 1106-1113.